Gait Effects of Unexpected and Coronally-Uneven Terrain on Healthy Adults

Kyle Harris Yeates

A thesis submitted in partial fulfillment of the
requirements for the degree of

Master of Science in Bioengineering

University of Washington
2014

Committee:

Glenn Klute
William Ledoux
Joan Sanders
Katherine Steele

Program Authorized to Offer Degree:
Bioengineering

University of Washington

Abstract

Gait Effects of Unexpected and Coronally-Uneven Terrain on Healthy Adults

Kyle Yeates

Chair of the Supervisory Committee:
Professor Joan Sanders
Bioengineering

In the United States, falls are the number one cause of death and injury in adults over the age of 65. Many of these falls occur in the mediolateral direction and are attributed to extrinsic factors, such as uneven terrain. This study explored the stability effects and biomechanical adaptations of 10 healthy adults during ambulation over unexpected and coronally-uneven terrain. Experiments were conducted on a custom built walkway with an integrated disturbance device that was nominally flush with the walkway, but could also produce unexpected 15° inversions and unexpected 15° eversions. Unexpected eversions had the largest destabilizing effect on participant gait, as measured by both the range of coronal angular momentum and the minimum inclination angle. The disturbed limb played a role in maintaining stability, as suggested by the time integral of the external coronal moment it provided to the body not being equal between all conditions. Contributing to the corrective moment of the disturbed limb were the coronal moments provided by the hip and ankle strategies, whose time integrals were also not equal between all conditions (expected flush, and unexpected inversion/eversion). A multi-segment foot model revealed asymmetric kinematic adaptations to the uneven terrain that could be related to anatomical features. The ankle joint (comprised of the subtalar and

tibiotalar joints) demonstrated more adaptation in the inversion than the eversion condition, as measured by the amount of inversion or eversion, respectively, of the hindfoot relative to the tibia in early and late-stance. By similar metrics, the midtarsal joint (comprised of the transverse tarsal and tarsometatarsal joints) demonstrated more adaptation in the eversion than the inversion condition. Kinetic adaptions of the ankle and midtarsal joints were significantly different between each of the conditions, but were not different for the grouped metatarsophalangeal joints. Like the disturbance itself, kinetic adaptations of the ankle and midtarsal joints were approximately equal and opposite for the inversion and eversion conditions. Clinically, the findings from this study suggest a sufficient coronal range of motion in the ankle joint is important for maintaining stability when ambulating over unexpected and coronally-uneven terrain; therefore, its preservation should be considered for certain orthopedic and prosthetic interventions as it may reduce the risk of patient falls.

Table of Contents

List of Figures

List of Tables

List of Equations

List of Abbreviations

AJ ..... Ankle Joint
ANOVA ..... One-Way Analysis of Variance
BH ..... Body Height
BM ..... Body Mass
COM ..... Center of Mass
COP ..... Center of Pressure
EVE or E ..... Eversion
ES ..... Early-stance
FF ..... Forefoot
FLU or F ..... Flush
GRF ..... Ground Reaction Force
HF ..... Hindfoot
HL1 ..... Heel
HX ..... Hallux
INV or I ..... Inversion
IQR ..... Interquartile Range
LL ..... Leg Length
LS ..... Late-stance
MPJ ..... Metatarsophalangeal Joint
MSFM ..... Multi-Segment Foot Model
MT1 ..... First Metatarsal
MT5 ..... Fifth Metatarsal
MTJ ..... Midtarsal Joint
RMSD ..... Root-Mean-Squared Deviation
ROM ..... Range of Motion
ST ..... Stance Time
WF ..... Whole Foot
WRT ..... With Respect To
WS ..... Walking Speed

Acknowledgements

I would like to thank Glenn Klute for his guidance and for the opportunity to work on fascinating and relevant research. I would also like to thank Ava Segal for her invaluable support in all aspects of this project, from experimental design to data interpretation. This work could not have been completed without the outstanding human participants and data processing work of Rose Kracht. Bil Ledoux and Eric Whittaker provided insightful foot expertise throughout the project. Janice Pecoraro coordinated all human participants recruitment and scheduling. Wesley Edmundson handled financing for the entire project.

This research was supported by the Department of Veterans Affairs, Rehabilitation Research and Development Service, grant A9243C.

Chapter I: Introduction

1.1 Background

In the United States, falls are the number one cause of death and injury in adults over the age of 65 [1]. Falls are nearly as prevalent in middle-aged individuals as they are in elderly populations [2]. Not only do falls cause physical injury, they also can have psychological effects, such as a fear of falling, which can lead to reduced mobility, independence, and quality of life [3]. In addition, it is estimated that the cost of falling in adults presently over the age of 65 will exceed 50 billion dollars by the year 2020 [3, 4].

The most common activity during a fall is walking [2], and a significant portion of these falls are attributed to extrinsic factors, such as uneven terrain [2, 5, 6]. Supporting this claim is the fact that both middle aged (40-59) and elderly (60-79) populations experience a majority of their falls outdoors (69%, and 75% of all falls, respectively) [2], where it is assumed that terrain is less predictable and less even. In outdoor falling, a significant portion of falls, around 25%, occur in the mediolateral direction [6]. It has also been shown that falls which occur outdoors are three times more likely to cause serious injury compared to those which occur indoors [7].

The study of falls and gait disturbances has thus far remained primarily focused on the sagittal plane, despite the prevalence of falls in the mediolateral direction [6]. In an attempt to advance the understanding of falls and gait disturbances, this study focused on exploring the mechanisms used by healthy individuals when adapting to gait disturbances in the form of coronally-angled uneven and unexpected terrain. The results of this work will shed light on how healthy adults adapt to coronally-uneven and unpredictable terrain, as well as help inform the development of prosthetic and orthopedic interventions so as to reduce the fall risk in patient populations who use these devices.

1.2 Previous Work

A fall is defined as an unexpected event in which an individual loses their balance and settles on the floor, or a lowered position [8]. Because falls are often injurious [2], and falls and balance are linked by definition, this study focused on disturbing the balance of participants, without making them fall.

Balance in gait, or gait stability, has been associated by a number of researchers with coronal plane kinetics and kinematics. Perhaps one of the most common measures of gait stability is step width variance [9], which suggests that higher step width variance is associated with less stability. Another metric used to analyze gait stability is the distance between the extrapolated center of mass (COM) and the boundary of an individual's base of support [10], in which a smaller value is associated with less stability. More recently, inclination angles have been used to evaluate stability in gait [11], in which a maximum inclination angle is associated with reduced stability. A closely related stability metric is the range of coronal angular momentum of an individual [12, 13], where a larger range of coronal angular momentum has been associated with reduced stability [12].

The existence of multiple stability metrics which focus on the coronal plane agrees well with research into the control mechanisms employed by humans during gait [14]. Kuo demonstrated that coronal plane motion in gait, unlike sagittal plane motion, which is passively stable, is unstable and requires active control from the central nervous system. It was proposed, and supported with test data, that in his experiment the body implemented a feedback system that used visual and vestibular inputs. As outputs, it was found that lateral stability was most effectively controlled by lateral foot placement (stepping strategy), followed by ankle inversion/eversion (ankle strategy), and hip abduction/adduction (hip strategy). Kuo's proposed inputs and outputs are consistent with the work of previously published research [15-19].

Studies of gait disturbances in the coronal plane have demonstrated that these strategies (stepping, ankle, and hip) are also used in disturbed walking. In the case of

unexpected inversions, studies have shown that participants employ the ankle strategy, as evidenced by activation of the peroneus longus and peroneus brevis muscles (which produce eversion moments about the ankle) [20, 21]. Lateral translational disturbances applied directly to the base of support of walking participants have evoked the use of the stepping and hip strategies, evidenced by alterations in step width and trunk angle [22, 23]. Lateral translational disturbances applied directly to the body of walking individuals also evoked stepping responses [10]. Smaller, localized disturbances in terrain, representative of external falling factors [5], also have evoked the use of the stepping and ankle strategies [24].

The aforementioned disturbance studies are all limited in that they treated the foot as a single rigid body; however, multiple studies have shown there exists movement between various segments of the foot [25-29]. Despite this, limited information is available on how a multi-segmented foot adapts to a non-flat surface. A study which used a multi-segment foot model (MSFM) to explore the kinematics of participants' feet as they walked across a cross-slope revealed that not only in the ankle joint, but also in the midtarsal joint, coronal plane angles were affected by the slope of the terrain [30]. While current findings suggest that there is motion between segments of the foot, the role this motion plays in recovery from discrete gait disturbances has yet to be defined.

Few studies have used a kinetic MSFM [31], as these models require a level of spatial resolution in the force sensing equipment that exceeds standard gait lab hardware. The proportionality assumption, which combines force measurements and pressure data, has recently been used to overcome this issue [26, 32]. The proportionality assumption assumes the ground reaction force (GRF) applied to each segment of the foot is identical in direction to that of the entire foot, but has a magnitude which is proportional to its fraction of the overall GRF (see section 2.4c for more detail). However, there exist no studies to date that use a MSFM to examine both the kinetics and kinematics of the foot as it adapts to discrete gait disturbances, such as unexpected and uneven terrain.

1.3 Purpose

The purpose of this study was to explore the stability effects and biomechanical adaptations of healthy adults as they walked over unexpected and coronally-uneven terrain. In addition, a kinetic MSFM was used to further explore the dynamics of the foot as it adapted to the coronally-uneven terrain. Adopting Bruening's MSFM [25, 33], this study divided the foot into three parts: the hindfoot, forefoot, and hallux sections. The tibia was connected to the hindfoot by the ankle joint (AJ), the hindfoot to the forefoot by the midtarsal joint (MTJ), and the forefoot to the hallux section by the metatarsophalangeal joint (MPJ) (see section 2.4b for more detail).

Data for this study were collected as participants walked across an experimental device that could produce an unexpected inversion/eversion disturbance (see section 2.2 for more detail). Participants and test devices were instrumented in such a way as to allow for the collection of both kinetic and kinematic data during the disturbance, as well as during the two preceding and two following steps. From this data, key metrics (see section 1.4 for more detail) were calculated to provide evidence for two biomechanical hypotheses (see section 1.5 and 1.6 for more detail).

1.4 Test Metrics

1.4a Stability

Performance metrics for stability in this study were based on recent findings which show that certain aspects of coronal plane motion can be used to differentiate between stable and unstable walkers [10-12].

In this study, the range of coronal angular momentum [12, 13] was used to evaluate the stability of participants during the disturbed gait cycle, and was calculated in Visual 3D (C-Motion, Germantown, USA). Specifically, in Visual 3D a model of each participant was made (see section 2.4 for more detail), and the coronal angular

momentum was the sum of the coronal angular momentum of each rigid body of the model about the COM of the entire model [12]. See ***Equation 1.***

$$\overrightarrow{L_{COM}} = \sum_{i=1}^{n}\left[\left(\overrightarrow{r_i^{COM}} - \overrightarrow{r_{body}^{COM}}\right) \times m_i \left(\overrightarrow{v_i^{COM}} - \overrightarrow{v_{body}^{COM}}\right) + I_i\overrightarrow{\omega_i}\right] \text{[12]}$$

Equation 1 - Angular momentum equation where $\overrightarrow{L_{COM}}$ is the angular momentum vector of the entire body model about its COM. $\overrightarrow{r_i^{COM}}$, $\overrightarrow{v_i^{COM}}$, and $\overrightarrow{\omega_i}$ are the position, velocity, and angular velocity vectors of the ith segment's COM. $\overrightarrow{r_{body}^{COM}}$ and $\overrightarrow{v_{body}^{COM}}$ are the position and velocity vectors of the body's COM. And m_i and I_i are the mass and moment of inertia of the ith segment. There are n=18 segments total in the model of the body used for this study. [12]

The only modification made to the range of coronal angular momentum metric was the start and end points of the gait cycle used to determine the range. Typically, the range of angular momentum is defined as the absolute value of the difference between the minimum and maximum values recorded between two consecutive heel strikes of the same limb. However, these bounds did not capture the full range of angular momentum induced by the disturbed step. In order to do so, the time period bounds of the gait cycle were modified. The modified time period bounds were the mid-stance of the non-disturbed limb on the step prior to the disturbance, and the mid-stance of the non-disturbed limb on the step after the disturbance. These bounds preserved the full gait cycle, and also captured the full range of coronal angular momentum induced by the disturbance (see ***Figure 1***).

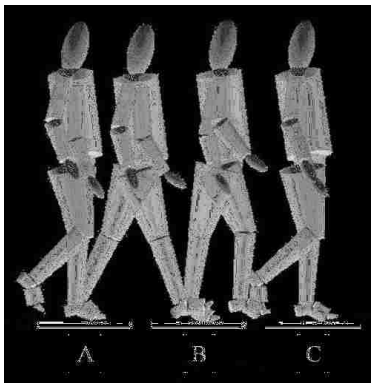

Figure 1 – Gait cycle used for range of coronal angular momentum calculation. Angular moment was evaluated between mid-stance of the (A) proceeding and (C) following steps. The disturbance device and disturbed step are located at (B).

The other stability metric used was the minimum inclination angle during single limb stance of the disturbed step. Inclination angle was defined as the angle between a vertical line, and a line from the COP to the COM [11] (see ***Figure 2***), and was calculated in Matlab (Mathworks, Natick, USA). Instead of using the maximum inclination angle as a metric, the minimum inclination angle was used. This decision was based on the fact that a smaller inclination angle would be closer to a negative inclination angle, which was considered unstable. A negative inclination angle was considered unstable because it would put the COM outside the base of support, as defined by the perimeter of the stance foot, which would likely result in significantly reduced stability [34]. The minimum inclination angle value was calculated within the single limb stance for two reasons: to avoid making COP assumptions during double limb stance, and because it had been previously shown that minimum inclination angles occurred during single limb stance [11].

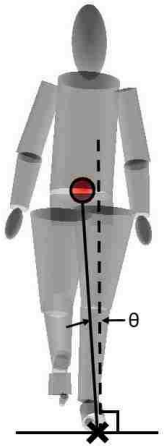

Figure 2 **-** Diagram of the inclination angle. Circle represents COM, X represents COP, dotted line represents a vertical line in the lab coordinate system, and θ represents the inclination angle.

1.4b Joint Moments and Angles

All kinetic and kinematic calculations were model based. Model specifics will be discussed in the modeling section (see section 2.4). All joint angles were calculated in Visual 3D according to the model's segment coordinate systems. Reported joint angle values correspond to the XYZ Euler angles used to rotate the distal segment to the proximal segment, with respect to the proximal segment's coordinate system. Per previous studies [35], joint angles were calculated at two key points in the stance phase of gait: early-stance (ES) and late-stance (LS). ES was defined as the time point during the first 50% of the stance cycle which had the highest vertical GRF, and LS was defined as the time point during the second 50% of the stance cycle which had the highest vertical GRF.

All joint moments were calculated in Visual 3D using an inverse dynamics approach. The iterative method used was based off established biomechanics principles [36, 37] and the exact algorithms can be found in the Visual 3D documentation [38].

Essentially, the joint reaction forces and joint moments were calculated from the most distal to the most proximal segments of the body by balancing forces acting on each segment using Newton's laws of motion. The following assumptions were made in the model: joint moments and forces were equal and opposite between the two segments of the joint; only gravity, external, and inertial forces were acting on each of the segments; each segment was rigid; the distal end of one segment was not equivalent to the proximal end of the adjacent distal segment. Reported joint moment values correspond to the moment acting about the joint on the distal segment, relative to the proximal segment's coordinate system.

1.4c Moment Integrals

The external coronal moments acting on the COM of the model caused by both the disturbed and contralateral limbs were calculated in Matlab. This was done by calculating the cross product of the GRF of the desired limb and the vector between the model COM and the COP of the desired limb.

Each of the external moments was integrated with the purpose of determining their effect on the range of the cType equation here.oronal angular momentum (see ***Equation 2***) for each trial. Because the range of coronal angular momentum within a gait cycle was used as the stability metric, the integration bounds were set as the mid-stance of the step prior to the disturbed step, and as the last point in the gait cycle that was used to calculate the range of coronal angular momentum for that particular trial (typically this point occurred at around the heel strike of the recovery step). Trapezoidal numerical integration in Matlab was used for all integral calculations.

$$\Delta L_{COM} = \int_{t1}^{t2} \sum_{i=1}^{n} M_{COM_i}\, dt$$

Equation 2 – Equation for change in angular momentum, where L_{COM} is the angular momentum of the model about the COM, and M_{COM_i} is the ith external moment acting on the model's COM. In the case of bipedal gate i=2.

The metric used to report joint moments was the time integral over the disturbed stance cycle. The integral was used in order to capture the entire effect of the joint moment, as this was thought to be the most relevant moment metric when considering the stability metrics used. Unfortunately, the time integral of the joint moments did not have as simple of a relationship to the range of coronal angular momentum when compared to the external moments. However, it was assumed the coronal moments of the joints of the disturbed limb contributed greatly to the external coronal moment acting on the COM caused by the disturbed limb, and therefore contributed to the stability metrics used. The same was assumed for the contralateral limb. All joint moment-time integrals were integrated using trapezoidal numerical integration in Matlab, using heel strike and toe off of the corresponding foot as integration bounds.

1.4d Step Width

To determine whether the stepping strategy of the disturbed limb was used, the step width of the step on to the disturbance device was calculated. It was calculated as the lateral distance (in the global coordinate system) between the heel marker of the contralateral limb at the heel strike prior to the disturbance, and the heel marker of the disturbed limb at the heel strike of the disturbance.

1.4e Normalization

In order to reduce variability between participants, normalization of various metrics was performed. Joint moments were normalized by body mass (BM), and leg

length (LL) [39]. Step width was normalized by LL. Joint moment-time integrals were normalized by BM, LL, and the length of time over which they were integrated (stance time (ST)). Angular momentums were normalized by BM, body height (BH), and walking speed (WS) [12]. It should be noted that none of the aforementioned normalizations significantly affected the results of the statistical tests conducted, but were retained in order to make comparisons with existing literature possible.

Joint angles were not normalized, but instead were shifted to account for the differences between participants' zero angle positions of the joints being analyzed. These differences arose from marker placement and boney landmark variation between each participant, which both affected segment orientations in the model. To accommodate for these variations, a correction factor was calculated for each joint of each participant. For the step onto the disturbance device, this value was the mean of the angle of the joint in question at heel-strike for each trial of the baseline condition (see section 2.1). This single constant was then subtracted from each point in the time series data for the joint in question for the step on to the disturbance device for all trials for that particular participant. The new zero angle position did not affect the magnitude of the range of motion (ROM), and also allowed for values of angles to be compared between participants.

Because both left and right foot dominant participants were tested, when necessary, left foot data was negated to match the polarity of the right foot. Such was the case for joint moments, joint moment integrals and joint angles. For all these data, the inversion direction was considered positive, and the eversion direction was considered negative.

1.4f Events

Three events were used for metric calculations, early-stance, mid-stance, and late-stance. Mid-stance was defined as the temporal midpoint between heel-strike and toe-off events of a single stance. Early-stance was defined as the point in time at

which the peak Z GRF occurred between the heel-strike and mid-stance. Late-stance was defined as the point in time at which the peak Z GRF occurred between mid-stance and toe-off [40].

1.5 Biomechanical Hypothesis I

Coronally-uneven and unexpected terrain disturbs human gait compared to walking on a flush surface. Reacting to this disturbance, the body uses mainly the ankle and hip strategies to help regain stability within the disturbed stance. Based on this hypothesis, the below supporting statements will be statistically tested, with the bolded hypothesis being the expected outcome.

The disturbance will affect participant stability. If so:

1.1) The range of coronal angular momentum about the COM of the body during the gait cycle corresponding to the disturbed step will be:

H0 = Equivalent for all conditions

H1.1a = Greater for inversion condition compared to flush

H1.1b = Greater for eversion condition compared to flush

1.2) The minimum of the inclination angle during single limb stance over the disturbed step will be:

H0 = Equivalent for all conditions

H1.2a = Less for inversion condition compared to flush

H1.2b = Less for eversion condition compared to flush

The ankle and hip strategies of the disturbed limb will mainly be used to recover from the disturbance. If so:

1.3) The time integral of the ankle coronal moment integrated over the stance period of the disturbed step will be:

H0 = Equivalent for all conditions

H1.3 = Not equivalent for all conditions

1.4) The time integral of the hip coronal moment measured over the stance period of the disturbed step will be:

H0 = Equivalent for all conditions

H1.4 = Not equivalent for all conditions

1.5) The width of the step on to the disturbance device, as defined by the lateral distance between the two heel markers as they strike the walking surface, will be:

H0 = Equivalent for all conditions

H1.5 = Not equivalent for all conditions

The use of correction strategies within the disturbed gait cycle will be primarily carried out by the disturbed limb. If so:

1.6) The time integral of the external moment (acting on the participant's COM) caused by the disturbed limb, integrated over the time period used to determine the range of angular momentum will be:

H0 = Equivalent for all conditions

H1.6 = Not equivalent for all conditions

1.7) The time integral of the external moment (acting on the participant's COM) caused by the contralateral limb, integrated over the period used to determine the range of angular momentum will be:

H0 = Equivalent for all conditions

H1.7 = Not equivalent for all conditions

1.6 Biomechanical Hypothesis II

When adapting to coronally-uneven and unexpected terrain, the foot acts as a multi-segmented system in which the ankle, midtarsal, and the metatarsophalangeal joints each adapt to the uneven terrain. Based on this hypothesis, the below supporting statements will be statistically tested, with the bolded hypothesis being the expected outcome.

The ankle joint will experience coronal angular motion, which will differ between the terrain conditions. If so:

2.1) Coronal angles between the hindfoot and tibia during the early single limb stance of the disturbed step will be:

H0 = Equivalent for all conditions

H2.1a = More positive for inversion compared to flush

H2.1b = More negative for eversion compared to flush

2.2) Coronal angles between the hindfoot and tibia during late single limb stance of the disturbed step will be:

H0 = Equivalent for all conditions

H2.2a = More positive for inversion compared to flush

H2.2b = More negative for eversion compared to flush

The midtarsal joint will experience coronal angular motion, which will differ between the terrain conditions. If so:

2.3) Coronal angles between the forefoot and hindfoot during early single limb stance of the disturbed step will be:

H0 = Equivalent for all conditions

H2.3a = More positive for inversion compared to flush

H2.3b = More negative for eversion compared to flush

2.4) Coronal angles between the forefoot and hindfoot during late single limb stance of the disturbed step will be:

H0 = Equivalent for all conditions

H2.4a = More positive for inversion compared to flush

H2.4b = More negative for eversion compared to flush

The midtarsal joint coronal moments will differ between terrain conditions. If so:

2.5) The time integral of coronal moments between the mid-foot and hind-foot during single limb stance of the disturbed step will be:

H0 = Equivalent for all conditions

H2.5 = Not equivalent for all conditions

The metatarsophalangeal joint coronal moments will differ between terrain conditions. If so:

2.6) The time integral of coronal moments between the toes and mid-foot during single limb stance of disturbed step will be:

H0 = Equivalent for all conditions

H2.6 = Not equivalent for all conditions

Chapter II: Methods

2.1 Experimental Design

2.1a Participants

10 healthy adult participants, with no self-reported musculoskeletal or gait disorders, were recruited for this study and completed all study procedures (age: 34.2±11.7 years, height: 1.76±0.09m, mass: 71.6±10.1kg, gender: 9 male/1 female). Each participant provided informed consent in accordance with the University of Washington Institutional Review Board (IRB) and the Veterans Administration Puget Sound Health Care System (VAPSHCS) IRB. This population was chosen to provide a performance baseline of the experimental device on the general, healthy adult population.

2.1b Procedure

The experiment was based on observing participants as they walked across an instrumented walkway, in the middle of which was a disturbance device capable of being positioned in a flush, inverted, or everted position (see ***Figure 3***). The condition of the disturbance device was capable of being blinded to the participants with the use of a thin opaque latex membrane that visually obscured its condition. A more thorough description of this device and the test equipment is given in section 2.2.

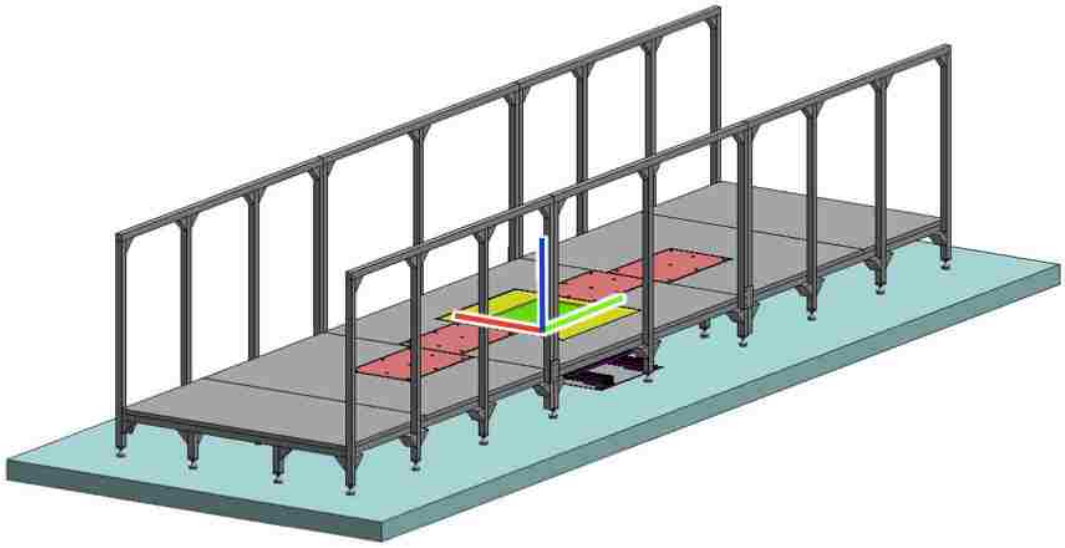

Figure 3 – Instrumented walkway and disturbance device. Force plate platforms shown in red, disturbance device shown in green/yellow, walkway floor and rails shown in grey, and lab floor shown in blue. Force sensing area of disturbance device shown in green. Global coordinate system shown at origin with Z-axis shown in blue, Y-axis shown in green, and X-axis shown in red.

All participants were outfitted with sensing equipment and black spandex clothing for the trials. Instrumentation included pressure sensing insoles worn inside shoes (see section 2.2), a mobile computer to collect the pressure data, and motion capture markers. In addition, all participants wore a pair of black spandex shorts and a black spandex shirt to optimize motion capture marker tracking. Shod walking was chosen for this experiment to most closely reproduce conditions that occur during a fall, as it was assumed that most falls on coronally-uneven terrain occur when the faller is wearing shoes. Participants reported being able to walk freely with the equipment on, and not feeling constrained by it. See ***Figure 4***.

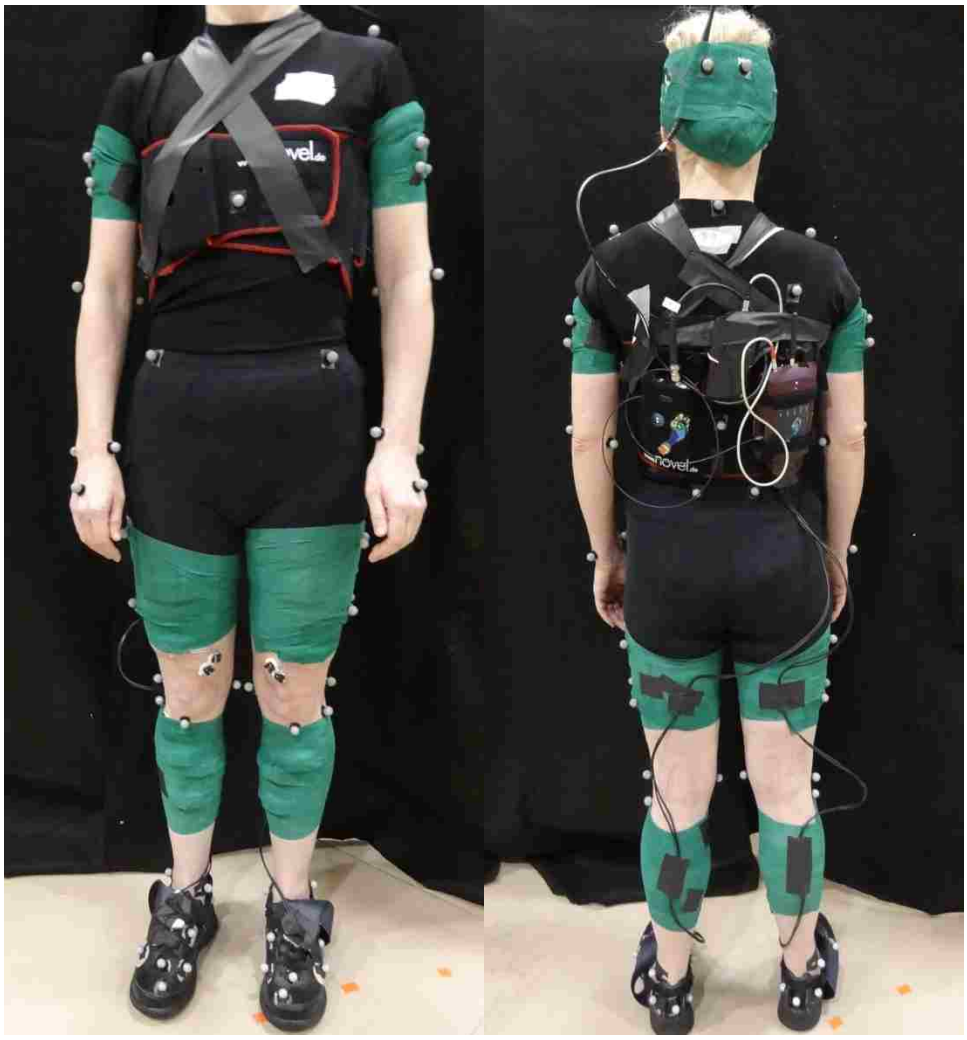

Figure 4– Fully instrumented participant, equipped with motion tracking and pressure sensing hardware.

Before walking trials began, static images and pressure sensor zeroing trials were collected. For static images, participants were asked to stand in the middle of the walkway and stand still for less than a one second period, during which their marker positions were recorded by the motion capture system, which were later used to build a rigid segment body model. Afterwards, participants were asked to sit on a chair, and lift their legs in order to unload their shoes so the pressure sensors could be zeroed.

To familiarize themselves with the walkway, participants were asked to walk across the walkway at a self-selected pace with the disturbance device in the flush, unblinded condition. They were instructed to have their self-reported dominant foot land on the center of the disturbance device. Participants typically landed on the disturbance device on their fifth heel strike from the starting position. Once participants were familiar with the walkway, and a starting point for their walking was established, the data collection began.

The first set of trials tested the unblinded flush, unblinded inverted, and unblinded everted positions. For the first five trials, the disturbance device was in the flush, unblinded condition. Once these trials were complete, the device was changed into the inverted, unblinded condition. The participants were again asked to walk across the walkway a few times to establish familiarity with the new position, and to establish a new starting point, if necessary, so their dominant foot would strike the disturbance device. Once this was done, the second five trials were collected. The device was then changed to the unblinded, everted condition, and the same procedure was repeated. After the unblinded trials were completed, participants were asked if they felt comfortable on the uneven terrain. If so, the experiment proceeded to blinded trials.

For the blinded trials, the condition of the disturbance device could not be seen by the participants, and was switched in a random order between each trial. Between trials, participants waited in a separate room, in which they could not observe the changing process. Once the changing process was complete, an opaque latex membrane was installed over the device to conceal its position. The participant would then be asked to come out of the room and walk across the walkway, always striking the disturbance device with their dominant foot. This process was repeated 15 times, five times for each position, which were presented to the participant in a random order.

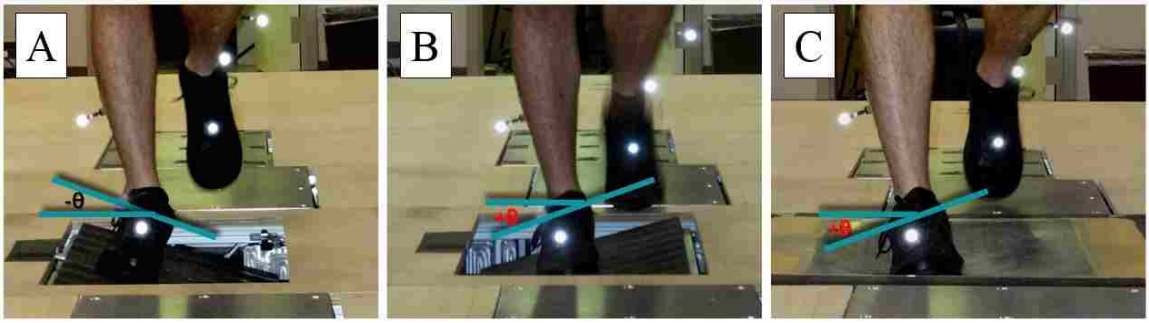

Figure 5 – Participant interacting with three different conditions of the disturbance device: (A) unblinded everted, (B) unblinded inverted, and (C) blinded inverted.

If blinded or unblinded trials were deemed unacceptable for any reason, such as participants missing force plates, additional trials were collected if time permitted in order to obtain the most complete data set possible for each participant.

2.2 Instrumentation

2.2a Walkway

An instrumented walkway was built with the purpose of producing unexpected and coronally-uneven disturbances similar to those that would be experienced outside in a natural environment (see ***Figure 3***). The disturbance mechanism chosen was a force plate that could be positioned flat and flush with the walkway, or could be rotated +/-15° in the coronal plane of the participant. The condition of the disturbance could be blinded from the user by installing an opaque latex membrane over the device.

The 15° angle of the disturbance was chosen based on a number of factors: safety, relevance, and adequacy. Determination of the angle began by creating prototype cross slope ramps ranging from 10-30°. Initial lab testing on the developers of the device revealed that 15° was large enough to disturb gait, especially when unexpected, but was not too large to cause falls or other injuries. Previous studies [20, 21] had applied unexpected inversions to participants during gait ranging from 25-30° with no reported

injuries, thus supporting that a 15° incline would be safe for participants in inversion. 15° of eversion was chosen for symmetry in the experiment. Informal surveys of uneven terrain found that on distressed sidewalks, grassy fields, and other common outdoor terrain, slopes of 15° existed.

The gross walking surface measured 6m long by 1.5m wide, with 1m high handrails along either side. The primary structure of the platform was extruded 6105-T5 aluminum beams with a cross sectional dimension of 40x40mm, and a floor made from two layers of 0.64cm thick plywood. The constructed platform was raised approximately 28cm above the surface of the lab floor to allow the disturbance device to remain below the walkway floor in all conditions.

2.2b Disturbance Device

The disturbance device, which was mounted in the middle of the walkway, consisted of four main components: the floor mount, the rotational base, the force plate assembly, and the floor panel (see ***Figure 6***).

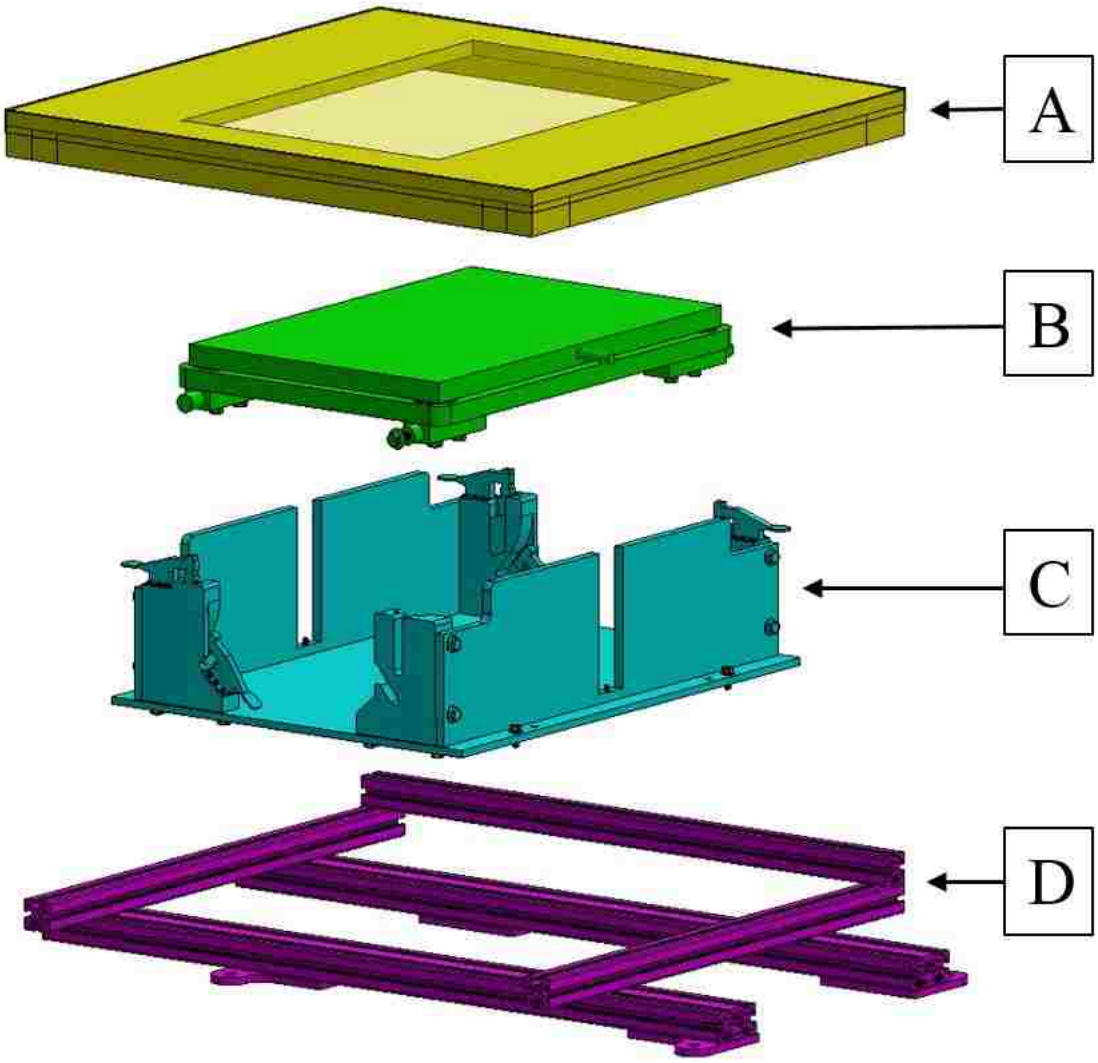

Figure 6 – Exploded view of disturbance device, consisting of: (A) floor panel, (B) force plate assembly, (C) rotational base, and (D) floor mount.

The purpose of the floor mount was to provide a surface upon which the rotational base could translate and be fixed upon; it also provided alignment features for the translation of the rotational base at each of its three positions: inverted, everted, and flush. The floor mount was a rigid structure of extruded 6105-T5 aluminum beams (cross sectional areas of 40x40mm and 40x80mm) with stainless steel 304 0H screw plates that enabled the entire disturbance device to be fixed to force plates that were mounted to the

lab floor. These force plates were not used for sensing, but instead only as a mounting surface. The floor mount's structure consisted of two main sliding rails, with two hard stops at each end, and an alignment bar.

The purpose of the rotational base was to consistently align and fix the force plate assembly into its three rotational positions. The rotational base consisted of a 1.25cm 304 0H stainless steel base upon which four 6061 T6 aluminum mounting brackets were fixed. These brackets each had cutouts to guide the location of the force plate assembly when being rotated into its three positions. In addition, three of the mounts were equipped with toggle clamps (1500 N holding force) to fix the force plate assembly once it was in the correct position. The fourth mount had slots, which mated with a M14 machine screw in the force plate assembly, thus providing fixation, without over-constraining the force plate assembly. Connecting the mounts were SUS 304 0H 1.25cm shear walls that provided additional rigidity to the system.

The purpose of the force plate assembly was to provide a rigid mounting surface for the force plate so that it could be adjusted into multiple rotational positions. The force plate assembly consisted of a Kistler 9286AA force plate (Kistler, Winterthur, CH), whose brass feet were each fastened to a 2.5cm thick slab of 6061 T6 aluminum. At each corner of this aluminum slab an aluminum 6061 T6 mounting block was attached. Each block featured a peg, which fit into its corresponding mounting bracket on the rotational assembly. One of the four pegs, which corresponded with the mounting bracket with no toggle clamps, housed a M14 machine screw that served as its fixation method.

The purpose of the floor panel was to ensure the participant stepped on the Kistler force plate (and not the surrounding hardware), and when desired, to blind the participant to the condition of the disturbance device. Two types of floor panels were used: one for the blinded condition, and one for the unblinded condition. Both had an extruded aluminum frame, upon which a 1.5cm plywood section was placed. The plywood had a 40x60cm rectangular cutout in the center, through which the user would step to contact the force plate. In the inverted and everted positions, in which the force plate was shifted,

an additional plywood piece was installed to ensure users could only step on the force plate (see ***Figure 7***). For blinded conditions, a floor panel section with a thin (0.2mm) and opaque latex membrane was used. This prevented participants from seeing the condition of the disturbance device. It was assumed the membrane did not impact gait, as forces produced by the membrane were negligible compared to those produced at the early-stance of gait.

Changing the positions of the disturbance device was a multi-step process, which took two technicians approximately two minutes to complete (see ***Figure 7*** for all three positions). The first step was to disengage each of the toggle clamps on the rotational device and to unscrew the one M14 screw on the force plate assembly. The force plate assembly could then be rotated to the desired position. Once this was done, the toggle clamps and screw were tightened. Then the screws attaching the rotational base to the sliding mount were loosened, and the rotational device was slid into its appropriate position. The inverted and everted positions were aligned using the hard stops, and the flush position was aligned using a 10cm spacer between either of the hard stops. Once the rotational base was slid, the screws connecting it to the floor base were re-tightened. Once completely adjusted, the newly positioned disturbance device was rigid.

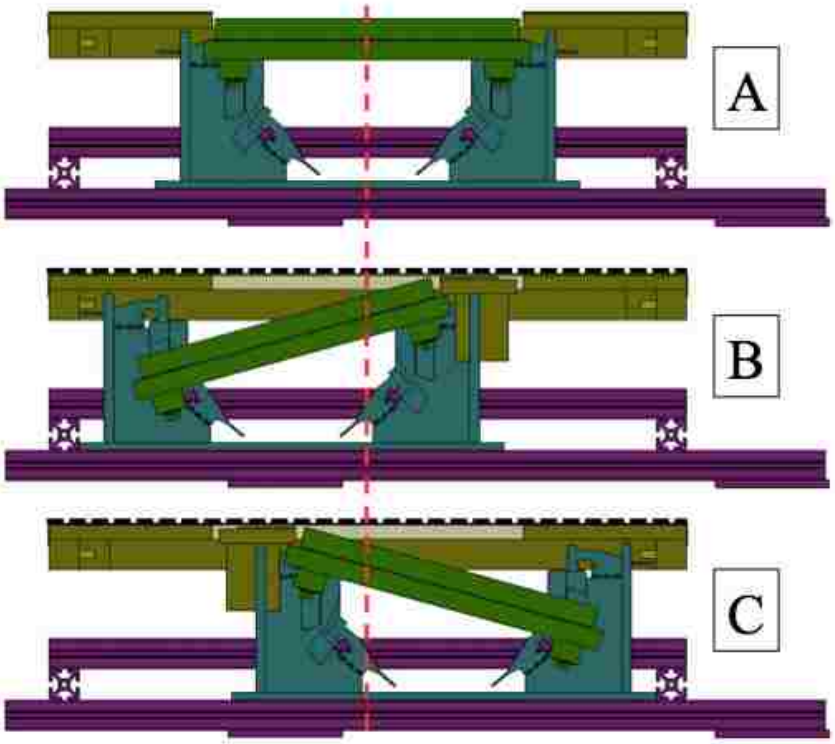

Figure 7 **-** Coronal plane cross sectional view of disturbance device in each position: flush (A), inverted (B), and everted (C). Nominal foot position of the participant is indicated by the vertical red dotted line. Flush position shown with floor panel without opaque latex membrane, while inverted and everted positions shown with floor panel with opaque latex membrane installed (shown as horizontal black dotted line).

Shifting the rotational device between positions was done to minimize the step down that participants experienced in the inverted and everted conditions. As seen in ***Figure 7***, the shift was used to bias the foot placement of the participants towards the upside of the force plate. Assuming participants stepped in the middle of the 40cm window opening of the floor panel, the step down for the flush condition was 0.7cm (considered negligible), and for the inverted and everted positions was 2.7cm.

2.3c Force Plate Platforms

In order to capture kinetics of the two steps preceding and the two steps following the step on the disturbance device, platforms were attached to four AMTI BP400600 (AMTI, Watertown, USA) force plates mounted on the lab floor which effectively raised their sensing surface 28.1cm to be flush with the rest of the walkway (see ***Figure 8***). The force plate platforms were mostly constructed from extruded 6051-T5 extruded aluminum bars with a cross sectional area of 40x40mm, and the walking surface was constructed from a 1.25cm thick 6061-T6 aluminum plate. The platforms were mounted to their respective force plates using hanger bolts.

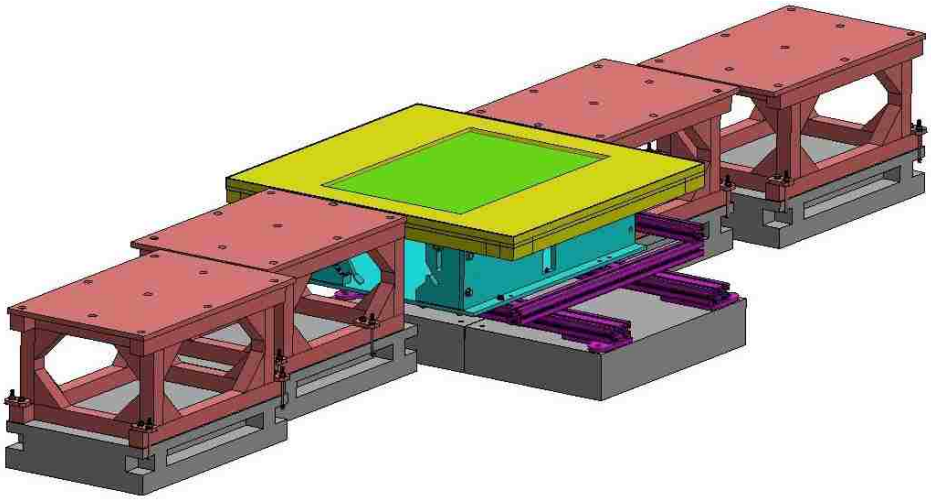

Figure 8 - View of force plate platforms, force plates, and disturbance device. Force plate platforms shown in red, force plates shown in grey. Note that the two force plates below the disturbance device were used strictly for mounting purposes.

2.3d Instrumented Shoes

A set of instrumented shoes were fabricated to allow for the motion capture and plantar pressure recording of the individual foot segments (see ***Figure 9***).

Figure 9 – Instrumented walking shoes with pressure sensing insoles installed.

To allow for motion capture of the individual segments of the foot within the shoe, multiple holes were cut from New Balance M577 walking shoes (New Balance, Boston, USA). These holes allowed the feet to be marked according to MSFM chosen for this study ([25], see Section XX), with the exceptions of the navicular and cuboid static markers, as the shoe could not be cut in those locations. These two markers were instead placed on the leather of the shoe, directly above the bony landmarks used to locate the navicular and cuboid bones. Because the midpoint of these markers were used to define the MTJ center, and the thickness of the shoe was equal on both sides, the effects of this modification were considered minimal. The markers placed on the feet were also used to track the motion of the pressure insoles, thereby allowing local coordinates of the pressure sensors to be associated with the lab's global coordinate system.

Plantar pressure recording was achieved using the Pedar Insole System (Novel, Munich, DE). This system consisted of a user-worn data transfer computer, a pair of pressure sensing insoles, and a wireless syncing system. Insole pairs were available in a

number of sizes to accommodate different shoe sizes, and were placed above the existing insoles of the shoe. Each sensing insole consisted of 99 capacitive pressure sensors, varying in size from 150-220mm^2. Data from these insoles was captured at a rate of 60Hz and sent wirelessly via Bluetooth to an operator-based computer that recorded the data. Syncing between the motion capture system and the Pedar system was achieved with the Pedar Wireless Syncing System.

2.3e Motion Capture System

A 12-camera Vicon motion capture system (Vicon Motion Systems, Oxford, UK) was used to record the positions of the retro-reflective markers placed on the participants. This system also contained a control unit, which handled the analog data acquisition from the force plate amplifiers, and also sent out the start signal to the Pedar wireless syncing system. Vicon Nexus software was used to record marker positions and force plate data for all trials. A 25N threshold was set for all force plate data.

Calculation of coronal moments, in comparison to sagittal moments, of the ankle are quite sensitive to errors in the distance between the joint center and the COP [41], therefore an additional calibration effort was made to reduce this error. The result was the use of an additional calibration step in which the origin and orientation of the lab coordinate system was determined from three markers which were placed at specific locations in the lab using machined aluminum fixtures. By using these additional fixtures, a high level of agreement between the motion capture system kinetics, and force plate kinematics was achieved. Please see section 2.5 for further details on validation.

2.3 Data Processing

Analog low-pass filters were applied to the outputs of the Kistler force plate of the disturbance device (100Hz cutoff frequency), and the AMTI force plates below the force plate platforms (1000Hz cutoff frequency used). Resonance tests were performed on the disturbance device as well as the force plate platforms by repeatedly striking their walking surfaces with a rubber mallet at various positions and angles to simulate heel

strikes. The force plate outputs were recorded at 1200Hz. It should be noted that due to the high cutoff frequency of the low-pass filter used on the AMTI force plates, peaks between 600-1000Hz would be folded about the Nyquist frequency of 600Hz and appear in the sampled data as peaks between 200-600Hz. Because the Kistler plate had a low-pass filter with a 100Hz cutoff, aliasing was not a concern. Spectral analysis in Matlab revealed that the percentage of the signal power existing below 25Hz was 90% for the AMTI force plates, and 85% for the Kistler force plate.

Digital filters were also used to process the data. Motion and force data were initially processed by Visual 3D, where a digital, 4^{th} order, single-pass bi-directional, low-pass, Butterworth filter was applied with cutoff frequencies of 25Hz for kinetic data, and 6Hz for kinematic data. The kinetic cutoff frequency was chosen in order to eliminate ringing artifacts from the force platforms and disturbance device, while still preserving the frequency content of standard gait [42]. The 6Hz cutoff frequency for kinematic data is based off the suggested value provided by Winter [37]. The Pedar insole data required no filtering, as the insoles have been shown to maintain a force-output/force-input ratio between 1.0-0.9 for frequencies between 0-150Hz [43] which encompasses those of standard gait.

Filtered kinetic and kinematic data were exported to Matlab, where they were combined with pressure data to calculate the individual foot segment GRFs and COPs. These individual foot segment forces were then applied to the MSFM in Visual 3D which used inverse dynamic calculations to produce joint moments.

2.4 Modeling

A modified Plug-In Gait model was combined with a MSFM to analyze whole body and multi-segment foot dynamics in a single model. The proportionality assumption was used to calculate GRFs for the individual segments of the foot.

2.4a Whole Body Modeling

Following previously established methods [36], a rigid segment, whole body model with six degree of freedom joints was developed based off the Vicon Plug-In Gait model (see ***Figure 10***). Modifications included the tracking of the femur, tibia/fibula, and humerus with the use of marker clusters [44]. Hip joint centers were calculated using the CODA method [45]. The mass of body segments were based off experimental data [46]. Another modification to the Plug-In-Gait model was the addition of multi-segment feet.

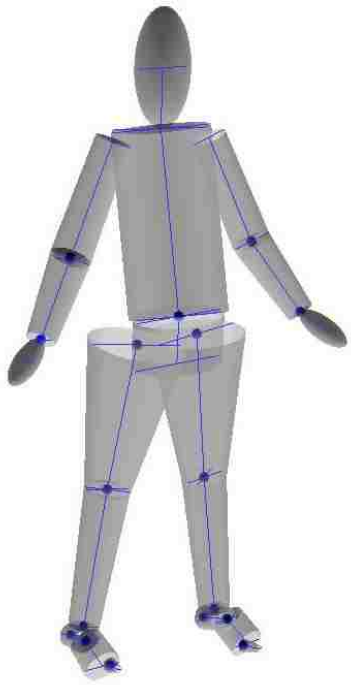

Figure 10 – Whole body model as seen in Visual 3D. Geometric representations of segment volumes shown as bodies. Lines represent segment axes, and dots represent joint locations.

2.4b Multi-Segment Foot Model

Each foot was modeled as three separate segments: the hindfoot, forefoot, and hallux section, according to Bruening's MSFM [25, 33]. The hindfoot bones consisted of the talus and calcaneus; the forefoot bones consisted of the navicular, cuboid, cuneiforms, and metatarsals; and the bones of the hallux section consisted of the proximal, distal, and intermedial phalanges (see ***Figure 11***).

From proximal to distal, the joints in the MSFM were: the ankle joint (AJ), which joined the tibia and the hindfoot; the midtarsal joint (MTJ), which joined the hindfoot and forefoot; and the metatarsophalangeal joint (MPJ), which joined the forefoot and the hallux section. The AJ and MTJ were each modeled as six degree of freedom joints, while the MPJ was modeled as a four degree of freedom joint, with three degrees of translation, and one degree of rotation in the sagittal plane.

The AJ consisted of two main anatomical joints: the tibiotalar joint, responsible for dorsiflexion and plantaflexion of the talus and calcaneus; and the subtalar joint, responsible for inversion and eversion of the calcaneus [47]. The MTJ consisted of two main functional joints: the transverse tarsal joint, and the tarsometatarsal joint [48]. The main anatomical joints of the MPJ were the metatarsophalangeal joints.

To maintain an anatomically meaningful orientation of the hindfoot, while also maintaining its proximal joint at the AJ and distal joint at the MTJ, a dummy segment was also needed in the model. This segment linked the AJ to the heel marker of the hindfoot, and was tracked with the same markers used to track the hindfoot, and was assigned a negligible mass. The result was that it had no relative motion with the hindfoot, and negligible inertial effects. It simply acted as a rigid extension of the hindfoot, transferring all forces and moments from the hindfoot directly to the AJ.

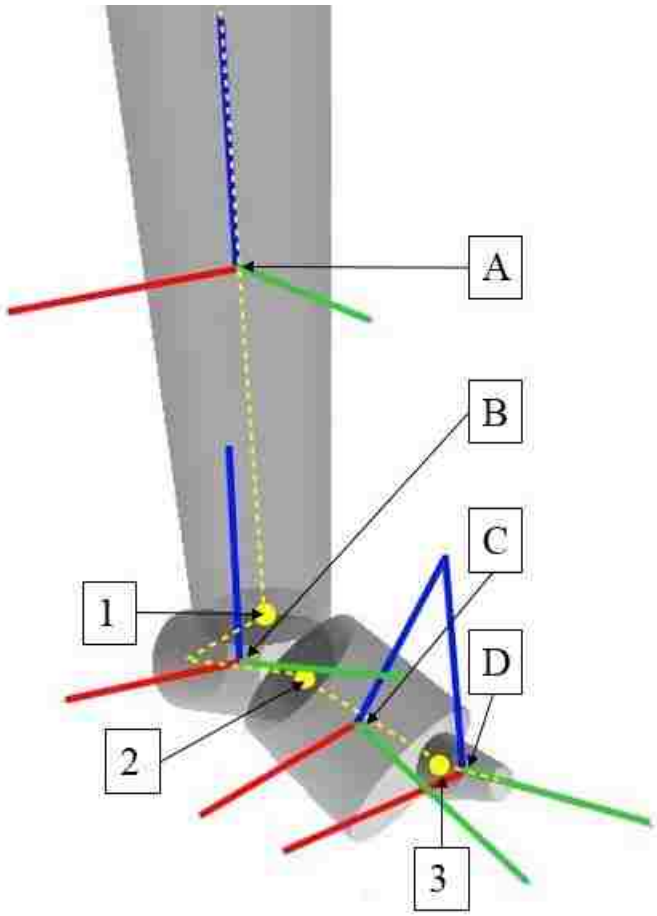

Figure 11 – Bruening MSFM [25] showing: (A) tibia, (B) hindfoot, (C) forefoot, and (D) hallux sections. Primary segment axes shown as dotted line, and are connected by joint centers for the (1) ankle joint (AJ), (2) midtarsal joint (MTJ), and (3) metatarsophalangeal joint (MPJ). Segment coordinate axis shown for each segment at their respective centers of mass. Z-axis shown in blue, Y-axis shown in green and X-axis shown in red.

Bruening's kinetic and kinematic MSFM was chosen due to its demonstrated repeatable and reliable kinetic and kinematic results for the complete stance phase of gait [31, 33]. It was also one of the few MSFM that could be adapted for use in shod walking. Other MSFMs had limitations that were not acceptable for this study. One such MSFM proposed by Dixon [49] could only be used after heel rise, which eliminated the

possibility of capturing early-stance dynamics, a key component of gait. Another model suggested by MacWilliams [26] had too many segment marking requirements to be adapted for shod walking, a key aspect of the experimental protocol for this study.

2.4c Proportionality Assumption

To produce MSFM kinetics, the proportionality assumption [26], which combined force and pressure data, was used to calculate the GRFs associated with individual foot segments. To implement the proportionality assumption, it was first necessary to mask the pressure sensing insoles into segments that corresponded with the segments of the MSFM. This was done by overlaying anatomical drawings of the foot over the pressure sensor array layout (see ***Figure 12***) to estimate which sensors would be assigned to the hindfoot, forefoot, and hallux sections. The masks defined using this visual approach were verified by palpation of the boney landmarks of participant feet as they stood on top of the pressure sensing insoles. The same mask definitions were used for all insole sizes.

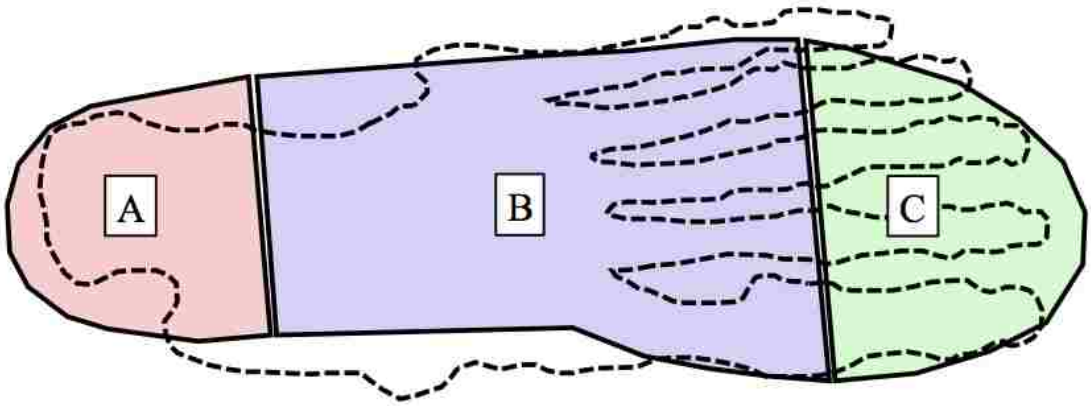

Figure 12 - Mask definitions for Pedar insole sensor array with outline of foot bones for general reference. (A) Insole sensors 1-26 were designated to the hindfoot, (B) sensors 27-75 were designated to the forefoot, (C) sensors 76-99 were designated to the hallux section.

The proportionality assumption used was that the GRF for each foot segment of the model could be approximated as a duplicate of the whole-foot GRF, with the exception that its force magnitude was a fraction of the whole-foot's force magnitude (see **Equation 3**). ***Figure 13*** shows a typical distribution of the vertical GRFs for each of the segments of the multi segment foot.

$$\left|\overrightarrow{F_S}\right| = \left(\frac{\sum_1^{n_S}\left|F_{S_i}\right|}{\sum_1^{n_W}\left|F_{W_i}\right|}\right)\left|\overrightarrow{F_W}\right| \quad \textbf{(A)}$$

$$\widehat{F_S} = \widehat{F_W} \quad \textbf{(B)}$$

Equation 3 - A). Proportionality assumption formula for magnitude ***B).*** Proportionality assumption formula for direction. $\overrightarrow{\boldsymbol{F_S}}$ is the force vector (with unit vector $\widehat{\boldsymbol{F_S}}$) being calculated and applied to a specified segment of the foot. $\overrightarrow{\boldsymbol{F_W}}$ is the force vector (with unit vector $\widehat{\boldsymbol{F_W}}$) of the entire foot, as recorded by the force plate. $\left|\boldsymbol{F_{S_i}}\right|$ is the force magnitude of the ith sensor in the segment mask of the foot which has $\boldsymbol{n_s}$ sensors total. $\left|\boldsymbol{F_{W_i}}\right|$ is the force magnitude of the ith sensor in the whole mask of the foot which has $\boldsymbol{n_w}$ sensors total. $\boldsymbol{F_{S_i}}$ and $\boldsymbol{F_{W_i}}$ were normal to the insole, and were the product of the ith sensors area and pressure as recorded by the insole sensor.

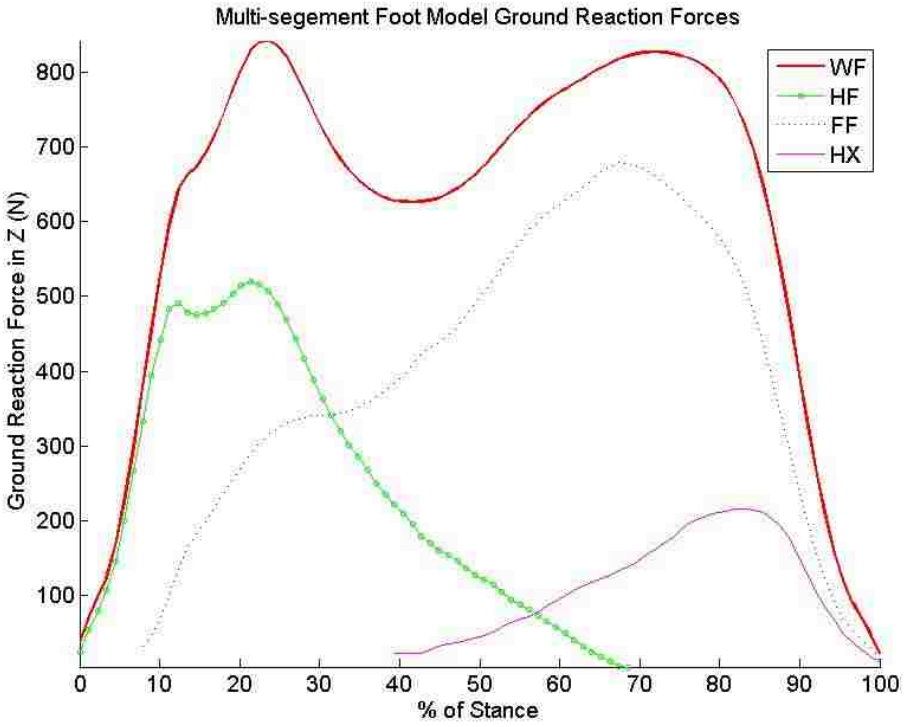

Figure 13 - Typical flat ground walking GRFs for each segment of the foot for whole foot (WF), hindfoot (HF), forefoot (FF), and hallux (HX) sections as recorded by the insole sensors. All forces were normal to the insole sensor, making them vertical (Z) in the global coordinate system. Body mass of participant was 92.3 kg.

The COPs for each of the foot segments were calculated by finding the centroid of the force for each of the segments. ***Figure 14*** shows a typical COP progression for a single flush, unblinded step for all segments compared to the whole foot.

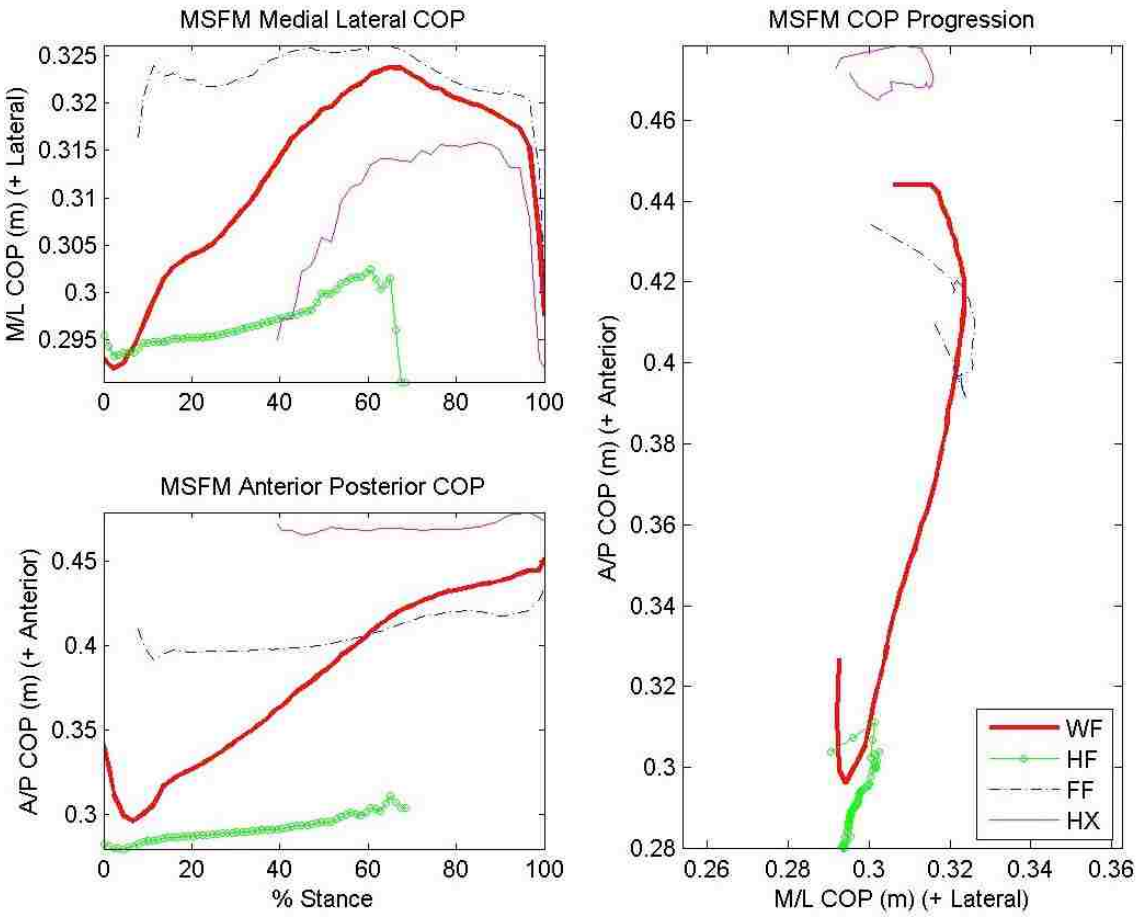

Figure 14 - Typical center of pressure (COP) paths for all segments of the foot compared to the whole foot for a flush, unblinded step. Labels are as follows: whole foot (WF), hindfoot (HF), forefoot (FF), hallux (HX), mediolateral (M/L), and anterior/posterior (A/P).

The COPs and force vectors for each segment of the foot were calculated relative to the insole coordinate system and were then transformed into the global lab coordinate system. This was accomplished by using the insole origin location and angle relative to the lab coordinate system, which were calculated in Visual 3D. Insole positions were tracked using the first metatarsal head (MT1), fifth metatarsal head (MT5) and heel (HL1) markers on the foot. The insole location relative to these markers was calculated from the model static image, where special markers were placed on the insoles, whose position were a known distance from the insole origin (see ***Figure 15***).

Figure 15 – Image of static markers used to locate the position of the insoles relative to the location of the feet markers. Markers defining position of insole circled in red.

By relating these insole markers to the MT1, MT5 and HL1 markers of the foot, the origin and angle of the sensor could be tracked throughout trials. Using these data, all MSFM COPs and force vectors were rotated using XYZ Euler angle rotation matrices, and then appropriately translated.

It should be noted that to address the issue of the insole bending throughout a stance cycle, the insole was assumed to be rigid, and to remain in a constant position, which was defined as its average position from 25-75% of the stance cycle. During this same time period, the position of the insole was adjusted to reduce the root-mean-squared deviation (RMSD) error between the insole and the force plate COP path. All pressure data was recorded at 60Hz, and up-sampled to 120Hz to match kinematic data.

2.5 Instrumentation Calibration and Validation

In order to ensure meaningful results, a series of calibrations and validations were performed on the test equipment and models used in this experiment. They are outlined below.

2.5a Force Plate Validation

Validation of the instrumented walkway was carried out by ensuring that each of the force plates produced accurate forces and COPs. This was done using the calibration pole technique [50]. This method used a pole equipped with tracking markers and a factory calibrated 1 kN load cell (Omegadyne, Sunbury, USA) whose orientation and tip position could be tracked using a Vicon Motion Capture System. The Vicon system simultaneously recorded the pole marker locations, pole load cell output, as well as force data from each of the force plates. Using Visual 3D it was possible to compare the COPs and force vectors produced by the force plates and by the calibration pole. Comparisons of COPs and force vectors were made at the four corners and the center of each of the static AMTI force platforms, as well as for the three positions of the Kistler plate on the disturbance device. At each location the pole was manually loaded for 10 seconds, starting at low (~100N) force, and peaking to a higher force of ~500N that incorporated up to 15° of off-vertical loading, before returning back to the low force. The validation test revealed good agreement between the calibration pole and force plate COP and force values (see
Table 1). Based on previous work showing <3mm of COP X error was acceptable for calculating coronal ankle moments [41], it was concluded that the accuracy of all force measurement devices was acceptable.

Validation Item	Disturbance Device Position			Static Force Plates			
	Flush	Inversion	Eversion	AMTI 1	AMTI 2	AMTI 4	AMTI 5
COP X RMSD (mm)	1.1±0.2	1.5±0.7	1.2±0.4	0.9±0.1	1.6±1.0	1.9±0.8	1.6±0.6
COP Y RMSD (mm)	3.3±0.5	3.5±0.6	3.7±0.7	2.9±1.4	3.6±0.4	1.6±0.3	1.4±0.5
FORCE X RMSD (N)	1.3±0.2	1.20±0.1	2.5±0.4	1.6±0.1	1.8±0.2	1.6±0.1	2.0±0.4
FORCE Y RMSD (N)	1.1±0.2	0.94±0.2	1.2±0.2	1.6±0.2	2.2±0.4	3.2±0.4	2.7±0.4
FORCE Z RMSD (N)	1.1±0.2	1.86±0.7	1.2±0.4	5.1±0.7	9.8±0.7	6.0±0.6	3.5±0.1

Table 1 - Validation results for COP and force for all force plates used. Mean±standard deviations of the RMSD between the calibration pole and force plate values. XYZ directions are from global coordinate system.

2.5b Insole Calibration

Prior to each data collection the Pedar insoles were calibrated using the Novel "TruBlu" calibration device. This process applied a set of uniform pressures, ranging from 0.1kPa to 6kPa, to the insoles, and associated the voltage output of each of the 99 sensors in each of the insoles to these specific pressures. Previous work [51] has shown this calibration procedure effective to the level of <2% error for loads of 500-1000N.

2.5c Multi-Segment Foot Model Split Plate Validation

The methods used in this study to calculate the COPs and GRFs for an in-shoe MSFM had not been previously used, therefore a two-part validation process was used to establish confidence in the method.

Part one tested the proportionality assumption when using the Pedar insole to measure the kinetics of a bare foot. This was achieved by fixing a calibrated Pedar insole over the split (~2mm) of two adjacent force plates. The insole was put in two positions, one in which the split aligned with the border of sensors used to define the hindfoot and forefoot (MTJ), and one in which the split was aligned with the border of the sensors used to define the forefoot and hallux (MPJ) (see ***Figure 16***).

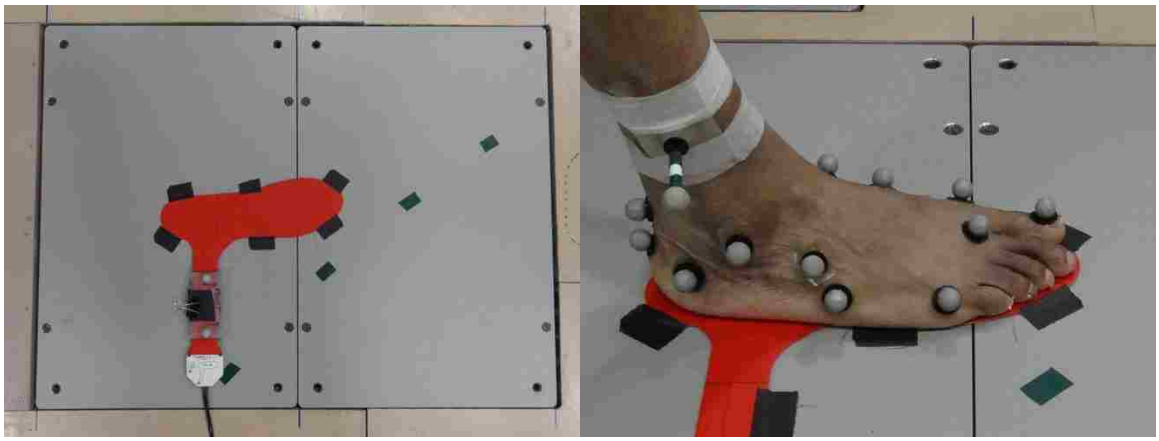

Figure 16 – Barefoot split plate validation technique. ***Left:*** Pressure sensing insole fixed between two force plates in a position to validate the MPJ. ***Right:*** Pressure sensing insole with a participant stepping on the insole.

Validation consisted of a consented and healthy participant being outfitted with reflective markers for the MSFM and taking targeted steps on the insole, which spanned adjacent force plates. 10 trials were collected for each of the two positions, in which the participant's foot only touched the insole. The same Visual 3D model was used to calculate the moments for each of the two joints using the standard split plate technique [33], and using the proportionality assumption technique. In the latter case, the force and COP outputs of the two adjacent force plates were combined in Visual 3D to produce a single COP and a single GRF [52], which was then combined with the pressure data (using the proportionality assumption) in order to produce the individual foot segment COPs and GRFs.

The moments calculated from Visual 3D using the two methods were then compared in Matlab. The resulting curves are shown in ***Figure 17*** which also displays the mean RMSD values (over the entire stance cycle) for each set of curves. There were eight successful trials for the MPJ, 10 successful trials for the MTJ, and both of these were also used for the AJ moment calculations.

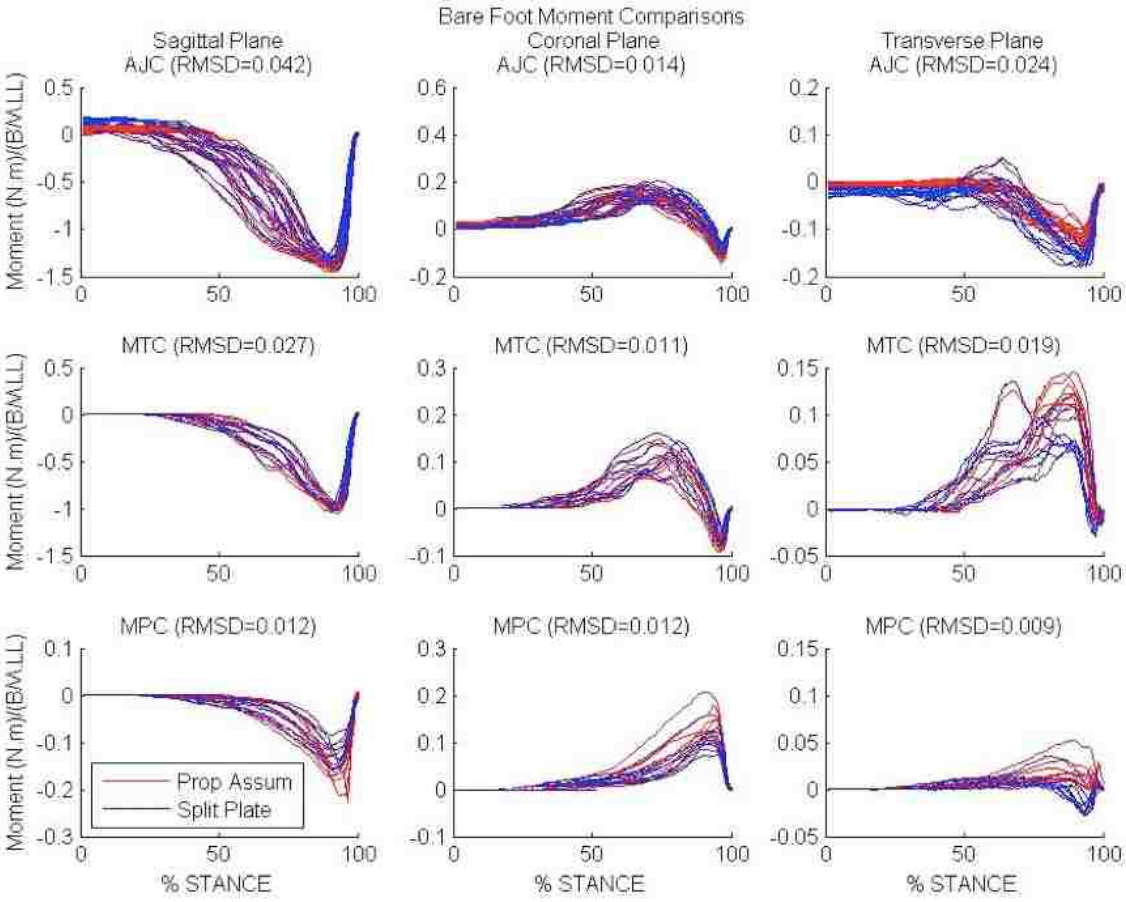

Figure 17– Barefoot comparisons between two MSFM moment calculation techniques for part one of the validation. Moments and RMSD values were calculated for AJ, MTJ, and MPJ in all three planes of motion. Moments normalized by body mass (BM) and leg length (LL).

Qualitatively, the shapes of the joint moments in the coronal and sagittal planes of motion agreed quite well between the two techniques, each sharing the same general shape and trend. In addition, the ranges of magnitudes for the moment curves were in agreement with previous literature on flat ground walking for the coronal plane [33]. Based on this, and the root-mean-squared deviation (RMSD) values being less than 10% of peak moment values for the coronal plane, it was determined that the proportionality

assumption held well in the coronal plane, when the Pedar insoles were mounted directly on the force plates.

Part two of the validation tested the proposed measurement technique in full. Not only was the proportionality assumption tested, but also the insole tracking method and the effect of mounting the insole inside of a shoe. This was achieved using a similar split plate technique to that of part one, with the exception that the participant was wearing the instrumented shoes as described in the section 2.3d. Wearing this shoe, and a marker set, the participant was asked to target their foot in two separate locations, one corresponding to the MTJ landing on the split, and one corresponding to the MPJ landing on the split (see ***Figure 18***). This was repeated until 10 clean strikes had occurred, in which the requested joint landed at the split of the plate, ensuring agreement between the mask definitions of the insole and the split plates.

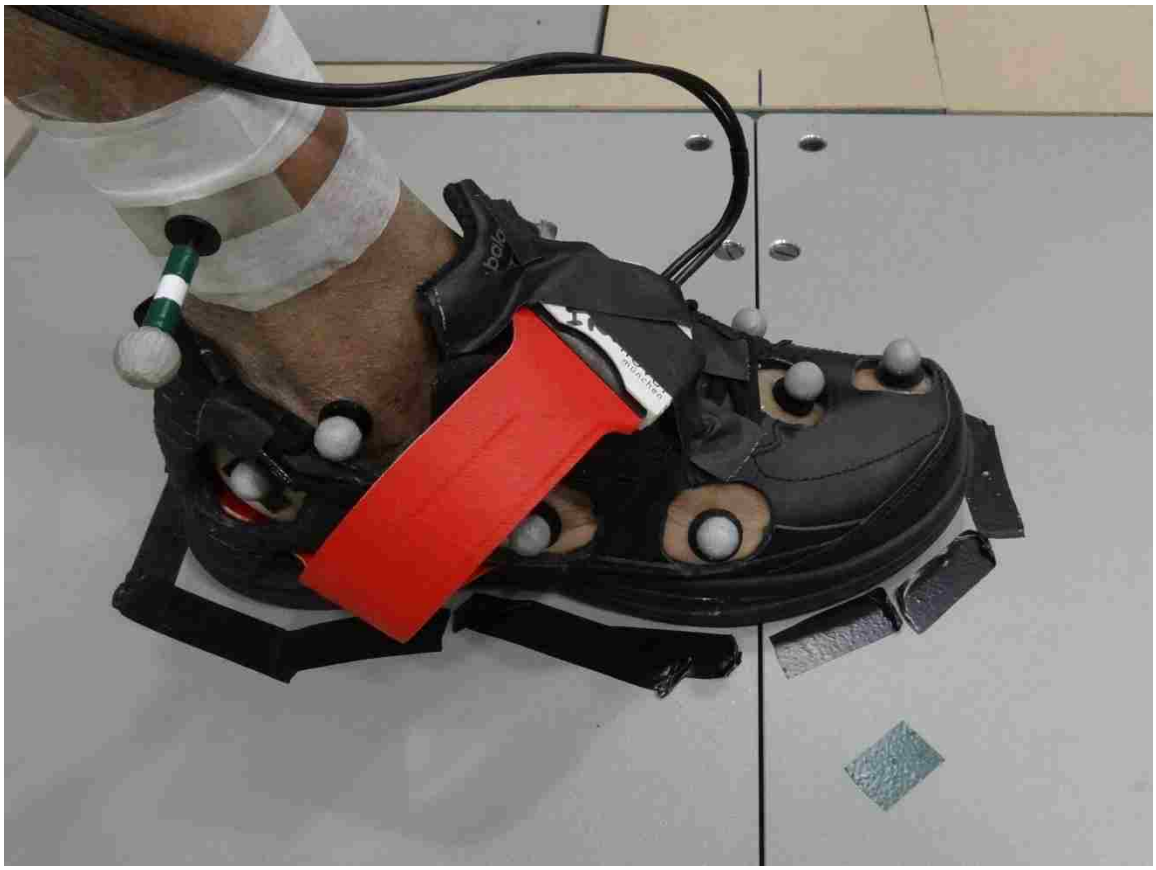

Figure 18 – Shod split plate validation technique. Participant in fully instrumented shoe is shown striking the split plates to validate the MPJ.

Using methods previously described to track the insoles and calculate the proportionality assumption, moments were calculated in Visual 3D for both the proportionality assumption as well as the split plate techniques. These moments were again compared in Matlab, and the resulting curves are shown in ***Figure 19***, which also displays the mean RMSD values (calculated over the entire stance phase) for each set of curves. There were eight successful trials for the MPJ joint, 10 successful trials for the MTJ, and both of these were also used for the AJ moment calculations.

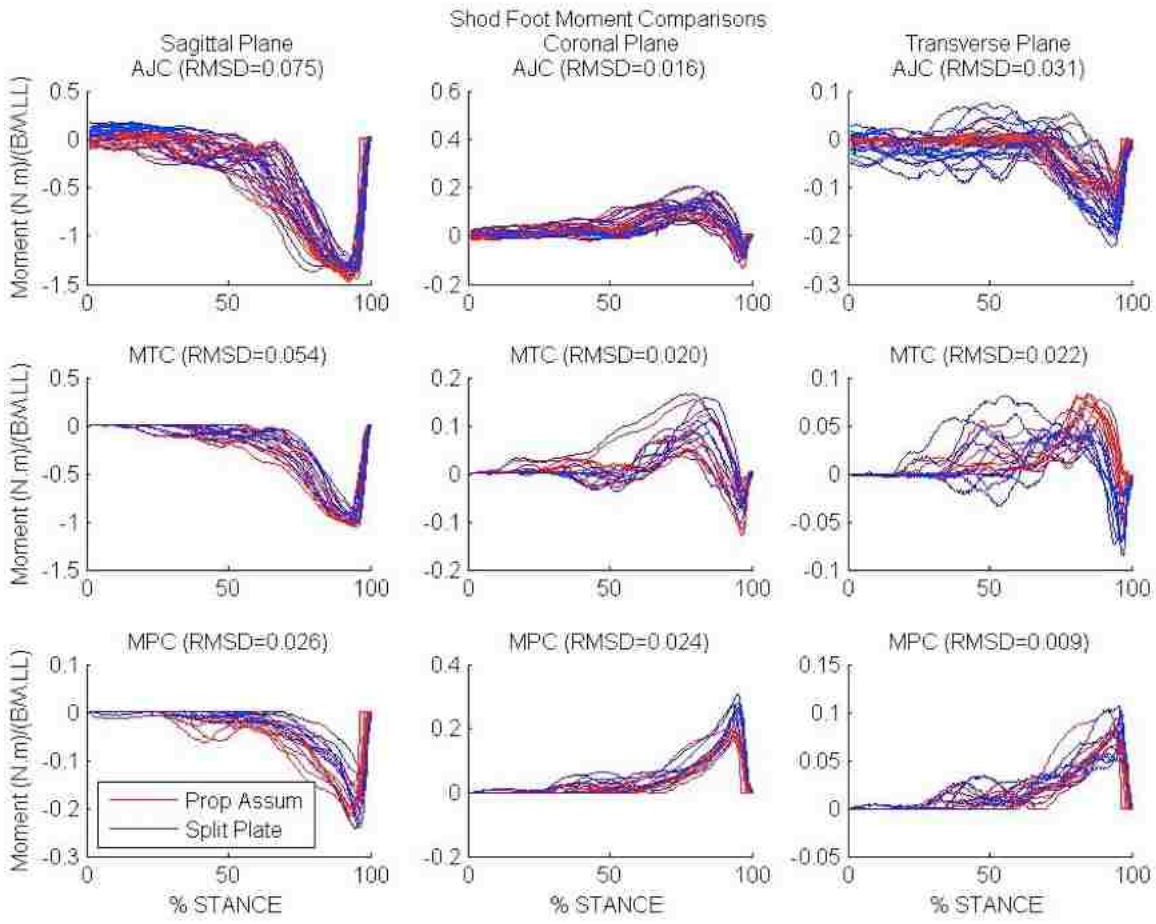

Figure 19– Shod comparisons between two MSFM moment calculation techniques for part two of the validation. Moments and RMSD values were calculated for AJ, MTJ, and MPJ in all three planes of motion. Moments normalized by body mass (BM) and leg length (LL).

RMSD values for part two moments are slightly higher than that of part one, yet still remain between 10%-15% of the peak moment values for all joints in the coronal plane. It is assumed that the additional error is a product of the pressure insole tracking as well as the existence of the shoe insole between the pressure sensor and the force plate. In addition to relatively low RMSD values, both methods have nearly identical curves for the coronal plane, suggesting that general behaviors and patterns of MSFM coronal moments could indeed be captured by the proportionality assumption method. Finally,

the ranges of magnitudes for the moment curves were in close agreement with previous literature for flat ground walking [33]. Based on these points, the measurement techniques proposed in section 2.4 were deemed acceptable.

2.5d Multi-Segment Foot Model to Whole Foot Model Verification

A verification was performed to ensure the use of a MSFM did not significantly affect test metrics which were measuring properties of the participants which were not MSFM dynamics. This was done by producing two models for each participant (N=10), both models were identical with the exception that one had multi-segment feet and used the proportionality assumption, while the other model had rigid feet and did not use the proportionality assumption. All test metrics used in biomechanical hypothesis I (which analyzed inclination angle, coronal angular momentum, and hip, ankle, and external coronal moments) were calculated for both types of models. For each metric, for each condition, a significant (alpha level = 0.05) difference was not discovered between the two model types. For this analysis, when the data being compared was normal, a two-sample t-test was used; when the data was not normal, a ranked sum test was used.

2.6 Statistical Methods

Each of the statistical hypothesis for biomechanical hypothesis I and II were tested using a Friedman's test, which is a non-parametric, repeated measures test [53]. This test was chosen over a repeated measures analysis of one-way variance (ANOVA) test due because the data did not meet the repeated measures ANOVA requirements [53]. It was decided to preserve the integrity of the data and not discard any outliers, as there was insufficient evidence to determine which points were outliers. In addition, log base 10, natural log, and power transformations were unable to normalize the data.

The Friedman test was performed on each metric using the Matlab statistical toolbox 8.3. One of the requirements of the Friedman test was that each participant/condition combination had to have the same number of repeated

measurements. The number of successfully recorded repeated measures varied from three to eight. As a result, the maximum number of repeated measures that were able to be used for statistical calculations was three. This requirement necessitated the selection of three repeated measures from any set of repeated measures with a length greater than three. This selection was done by random permutation, as to avoid introducing bias into the analysis.

If significance was detected at an alpha level of 0.05 for the Friedman test, a post-hoc multiple comparison test was performed to determine whether significant differences existed between each of the conditions. This was done by comparing conditions using individual Wilcoxon signed-rank tests, with a Bonferroni correction for the three conditions, and an alpha level of 0.05 [53].

Chapter III: Results

12 study participants were consented for the experimental procedure, but due to instrumentation error, full collections were only performed on 10 participants. 9 of the 10 participants were right foot dominant. 9 of the 10 participants were men. The means and standard deviations of the age, height, and mass of the participants were: 34.2±11.7 years, 1.76±0.09m, and 71.6±10.1kg, respectively. Only trials in which the participant cleanly struck the adjustable force plate, as well as the immediately preceding and following force plate were analyzed. A clean strike was defined as the entire foot of the participant landing inside the border of the force plate. None of the participants tripped or fell during the procedure; however, occasionally a participant's toe would scrape the edge of the walkway as they were stepping off the disturbance device. Trials in which this occurred were not used.

Only results for three of six conditions tested are reported. These are unblinded flush, blinded inverted, and blinded everted. Unblinded flush served as the baseline condition for normal gait, whereas blinded inversion and eversion represented unexpected, and coronally-uneven terrain, which was assumed to be a likely cause of mediolateral falls outdoors.

3.1 Biomechanical Hypothesis I Results

Statistical test results of performance metrics are shown in ***Table 2*** and in general, support biomechanical hypothesis I, which was: "Coronally-uneven and unexpected terrain disturbs human gait compared to walking on a flush surface." Reacting to this disturbance, the body uses mainly the ankle and hip strategies to help regain stability within the disturbed stance." Both stability metrics exhibited a significant pairwise difference between the eversion and flush condition, as seen in ***Table 2*** rows one and two, which correspond to ***Figure 20*** and ***Figure 21***, respectively. Significant pairwise differences were found between all conditions for the ankle coronal moment-time integral, as seen in ***Table 2*** row three, which corresponds to ***Figure 22***. The hip coronal moment-time integral was not equal between all conditions, and a significant pairwise difference between inversion and eversion conditions was detected, as seen in ***Table 2*** row four, which corresponds to ***Figure 23***. Similarly, the external coronal moment-time integral of the disturbed limb was also not equal between all conditions, and a significant pairwise difference between inversion and eversion conditions existed, as seen in ***Table 2*** row five, which corresponds to ***Figure 24***. Results did not support that the external coronal moment-time integral of the contralateral limb was not equal between conditions, as seen in ***Table 2*** row six, which corresponds to ***Figure 25***. Results also did not support that the step width on to the disturbance was not equal between conditions, as seen in ***Table 2*** row seven, which corresponds to **Figure 26**.

Metric	Units	P-Value	Median (IQR)			Pairwise Differences		
			Flush	Inversion	Eversion	F to I	F to E	I to E
Range of Coronal Angular Momentum	$\frac{N \cdot m \cdot s}{BM \cdot BH \cdot WS}$	< 0.001	0.03(0.01)	0.03(0.01)	0.04(0.01)	No Sig Diff	F < E	I < E
Minimum Inclination Angle	Degrees	< 0.001	2.88(0.90)	2.54(1.11)	2.34(0.94)	No Sig Diff	F > E	No Sig Diff
Ankle Coronal Moment-Time Integral	$\frac{N \cdot m \cdot s}{BM \cdot LL \cdot ST}$	< 0.001	-0.03(0.14)	-0.20(0.09)	0.11(0.13)	F > I	F < E	I < E
Hip Coronal Moment-Time Integral	$\frac{N \cdot m \cdot s}{BM \cdot LL \cdot ST}$	< 0.001	-0.56(0.11)	-0.60(0.21)	-0.41(0.26)	No Sig Diff	No Sig Diff	I < E
External Coronal Moment-Time Integral of Disturbed Limb	$\frac{N \cdot m \cdot s}{BM \cdot LL \cdot ST}$	< 0.001	-0.16(0.03)	-0.12(0.03)	-0.22(0.09)	No Sig Diff	No Sig Diff	I > E
External Coronal Moment-Time Integral of Contralateral Limb	$\frac{N \cdot m \cdot s}{BM \cdot LL \cdot ST}$	0.371	0.07(0.03)	0.07(0.02)	0.07(0.02)	No Sig Diff	No Sig Diff	No Sig Diff
Step Width	m / LL	0.236	0.14(0.03)	0.13(0.04)	0.13(0.04)	No Sig Diff	No Sig Diff	No Sig Diff

Table 2 - Statistical results for biomechanical hypothesis I. P-values based on Friedman test. Pairwise differences based on Wilcoxon signed-rank tests, with a Bonferroni correction, and an alpha level of 0.05. Metrics normalized to body mass (BM), body height (BH), walking speed (WS), leg length (LL), and stance time (ST). Median and interquartile range (IQR) reported due to non-normal nature of metrics.

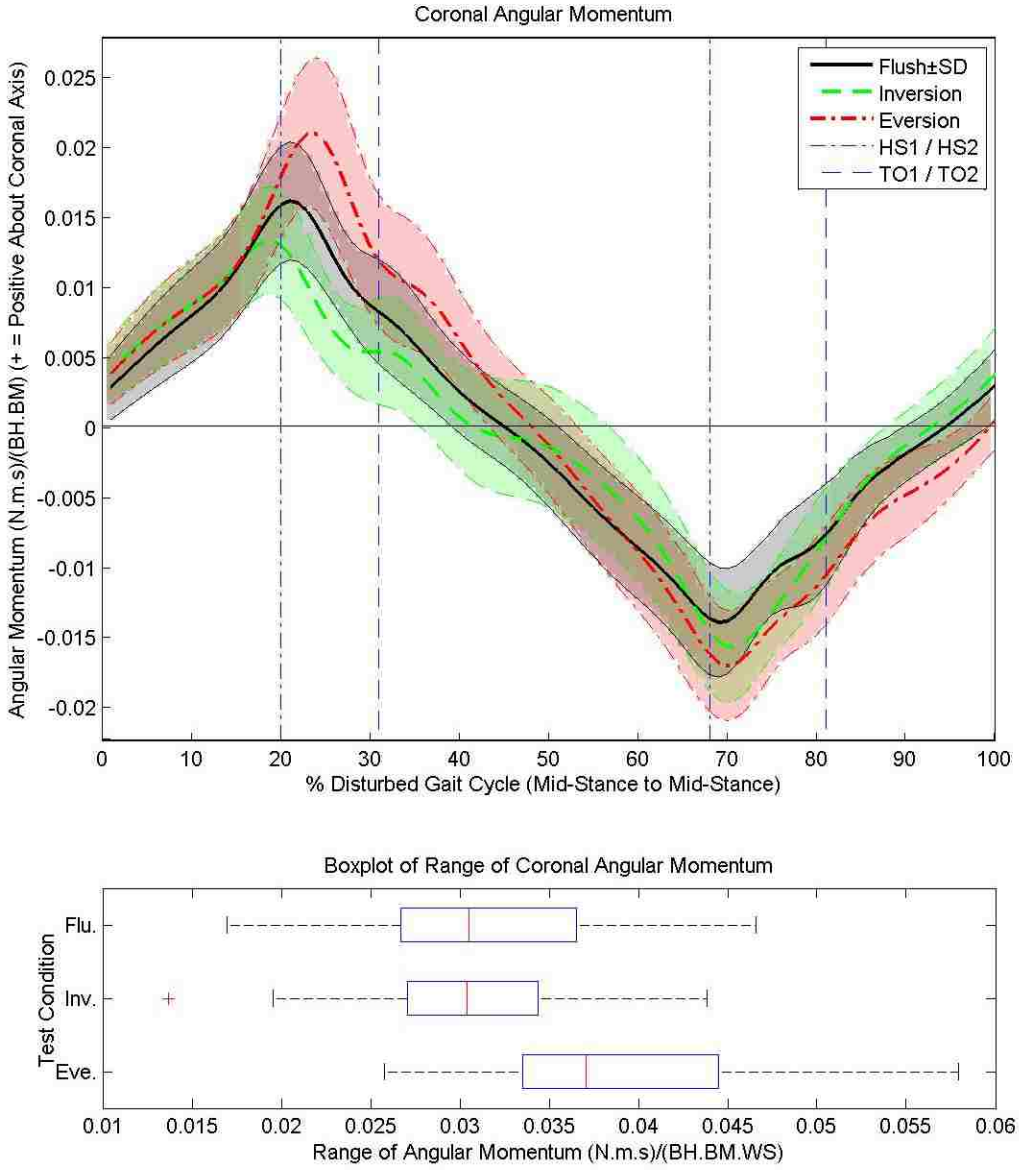

Figure 20 **–** ***Top****:* Time series of mean coronal angular momentum for each condition plotted over the disturbed gait cycle. Mean and standard deviation lines are for all trials for all participants. ***Bottom****:* Boxplot of range of coronal angular momentum. Time series and boxplot data normalized to body mass (BM), body height (BH), and walking speed (WS). Vertical lines represent the first and second heel strike (HS) and toe off (TO) events to occur in the disturbed gait cycle. Events are average values for all participants for all conditions.

Related to biomechanical hypothesis 1.1, these results reject the null hypothesis, and support the alternative hypothesis that the range of coronal angular momentum was not equivalent for all conditions, and was significantly greater for the everted condition compared to the flush condition. This can be seen in row one of ***Table 2*** and ***Figure 20***. These results suggest that the disturbance did affect the stability of the participants, and that the eversion condition had the largest destabilizing effect on gait stability. However, there was no detectable difference in the range of coronal angular momentum between the inversion and flush condition, suggesting the inversion condition did not have as large an effect on gait stability as the eversion condition.

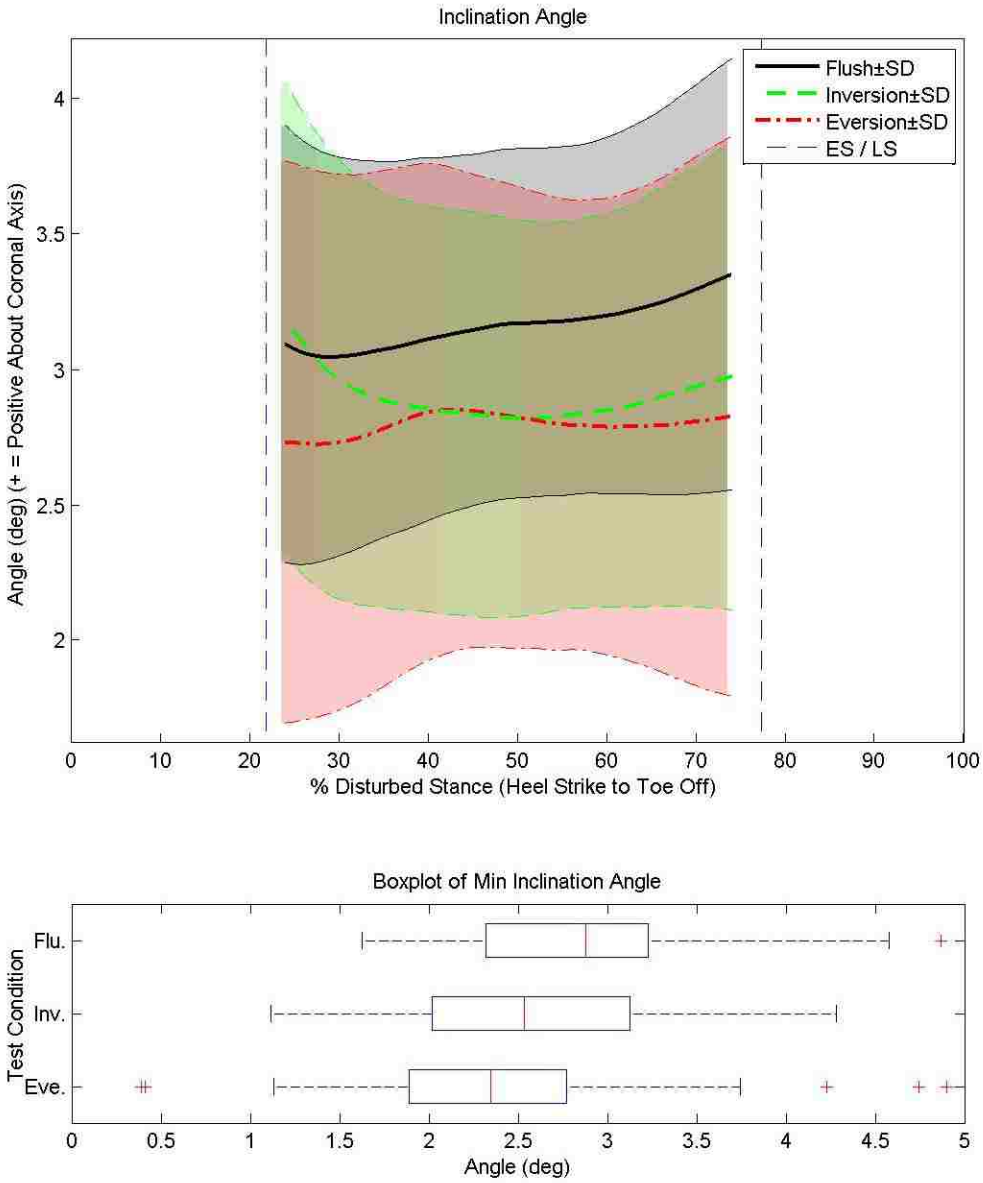

Figure 21 – ***Top****:* Time series for mean inclination angle for each condition plotted over the disturbed stance. Inclination angle only plotted for single limb support. Mean and standard deviation lines are for all trials for all participants. Vertical dotted lines indicate average early-stance (ES) and late-stance (LS) time points. ***Bottom****:* Boxplot of minimum inclination angle for each condition.

Related to biomechanical hypothesis 1.2, these results reject the null hypothesis, and support the alternative hypothesis that the minimum inclination angle was not equivalent for all conditions, and that the eversion condition had a significantly smaller inclination angle compared to the flush condition. This can be seen in row two of ***Table 2*** as well as ***Figure 21***. Similar to the range of coronal angular momentum, these results suggest that the disturbance did affect the stability of the participants, and that the eversion condition had the largest destabilizing effect on gait stability. However, there was no detectable difference in the minimum inclination angle between the inversion and flush condition, suggesting the inversion condition did not have as large an effect on gait stability as the eversion condition.

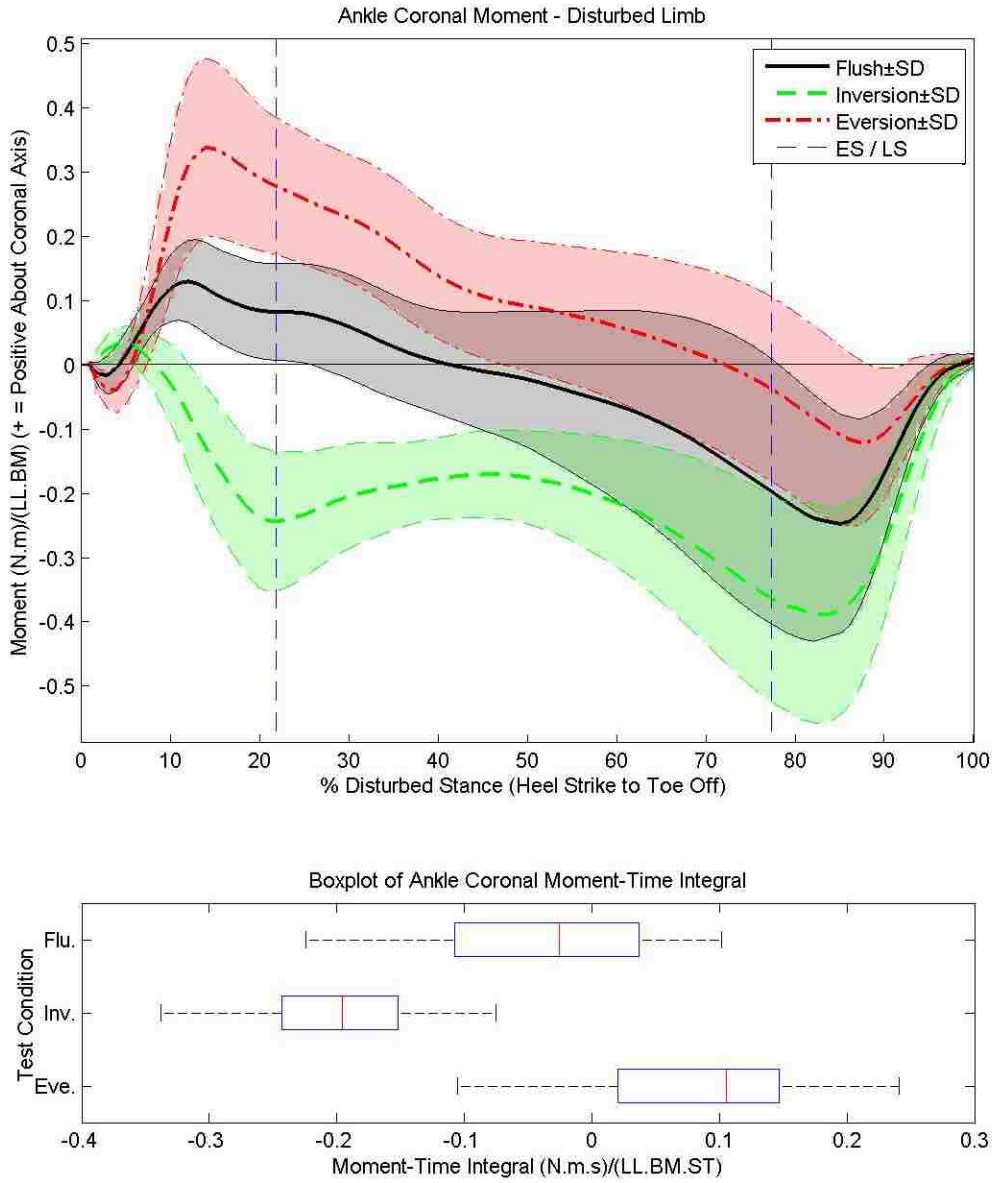

Figure 22 – Top: Time series for mean ankle coronal moment for each condition plotted over the disturbed stance. Mean and standard deviation lines are for all trials for all participants. Vertical dotted lines indicate average early-stance (ES) and late-stance (LS) time points. ***Bottom:*** Boxplot of ankle coronal moment-time integral. Time series and boxplot data normalized to body mass (BM), leg length (LL), and stance time (ST).

Related to biomechanical hypothesis 1.3, these results reject the null hypothesis, and support the alternative hypothesis that the time integral of the ankle coronal moment was not equivalent for all conditions, and that it was significantly more negative for the inversion condition compared to the flush condition, and was significantly more positive for the eversion condition compared to the flush condition. This can be seen in row three of ***Table 2*** as well as ***Figure 22***. These results suggest that the ankle strategy was used for both disturbance conditions, and that the ankle coronal moments were affected by each of the disturbance conditions. Both eversion and inversion curves are clearly separated from the flush condition in ***Figure 22*** with this difference being the most pronounced at early-stance for eversion. Throughout stance the inversion case had a more negative moment when compared to the other two conditions, and the eversion case had a more positive moment compared to the other two conditions.

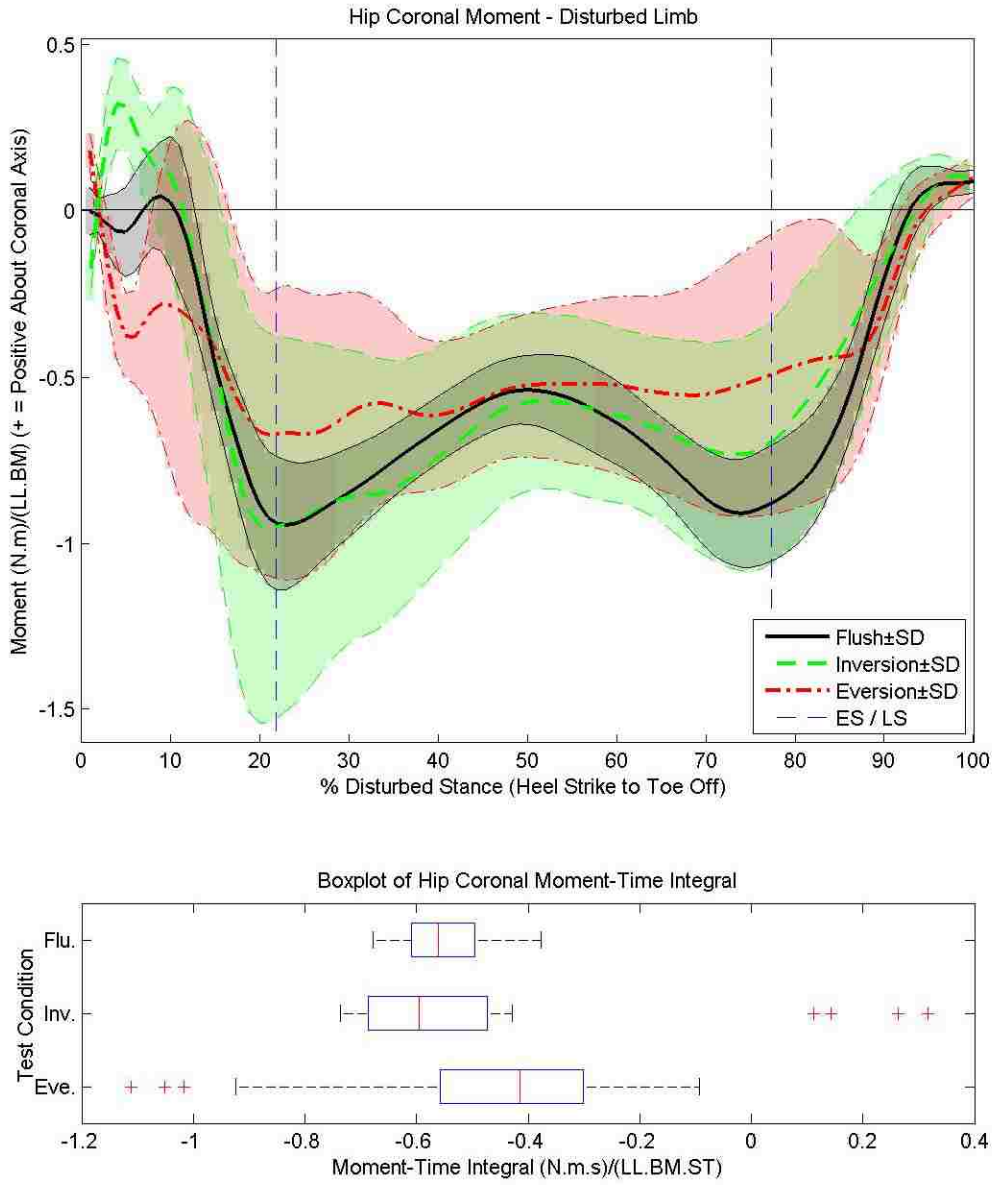

Figure 23 **–** ***Top:*** Time series of hip coronal moment for each condition plotted over the disturbed stance. Mean and standard deviation lines are for all trials for all participants. Vertical dotted lines indicate average early-stance (ES) and late-stance (LS) time points. ***Bottom:*** Boxplot of hip coronal moment-time integral. Time series and boxplot data normalized to body mass (BM), leg length (LL), and stance time (ST).

Related to biomechanical hypothesis 1.4, these results reject the null hypothesis, and support the alternative hypothesis that the time integral of the hip coronal moment was not equivalent for all conditions. This can be seen in row four of ***Table 2*** as well as ***Figure 23***. The eversion condition had a significantly more positive time integral than the inversion condition. These results suggest that the hip strategy was used, and that its use differed between conditions. No significant difference was detected between the inversion and flush conditions and the eversion and flush conditions. However, in viewing the time series plot and boxplot of ***Figure 23***, it can be seen that the time integral of the hip moment for the eversion condition was generally more positive than the flush condition. In addition, the eversion condition and had less defined peaks at early-stance and late-stance when compared to the flush and inversion conditions. A significant difference may not have been detected between the flush and eversion conditions due to the high variance of this metric. The observed outliers were from a single subject.

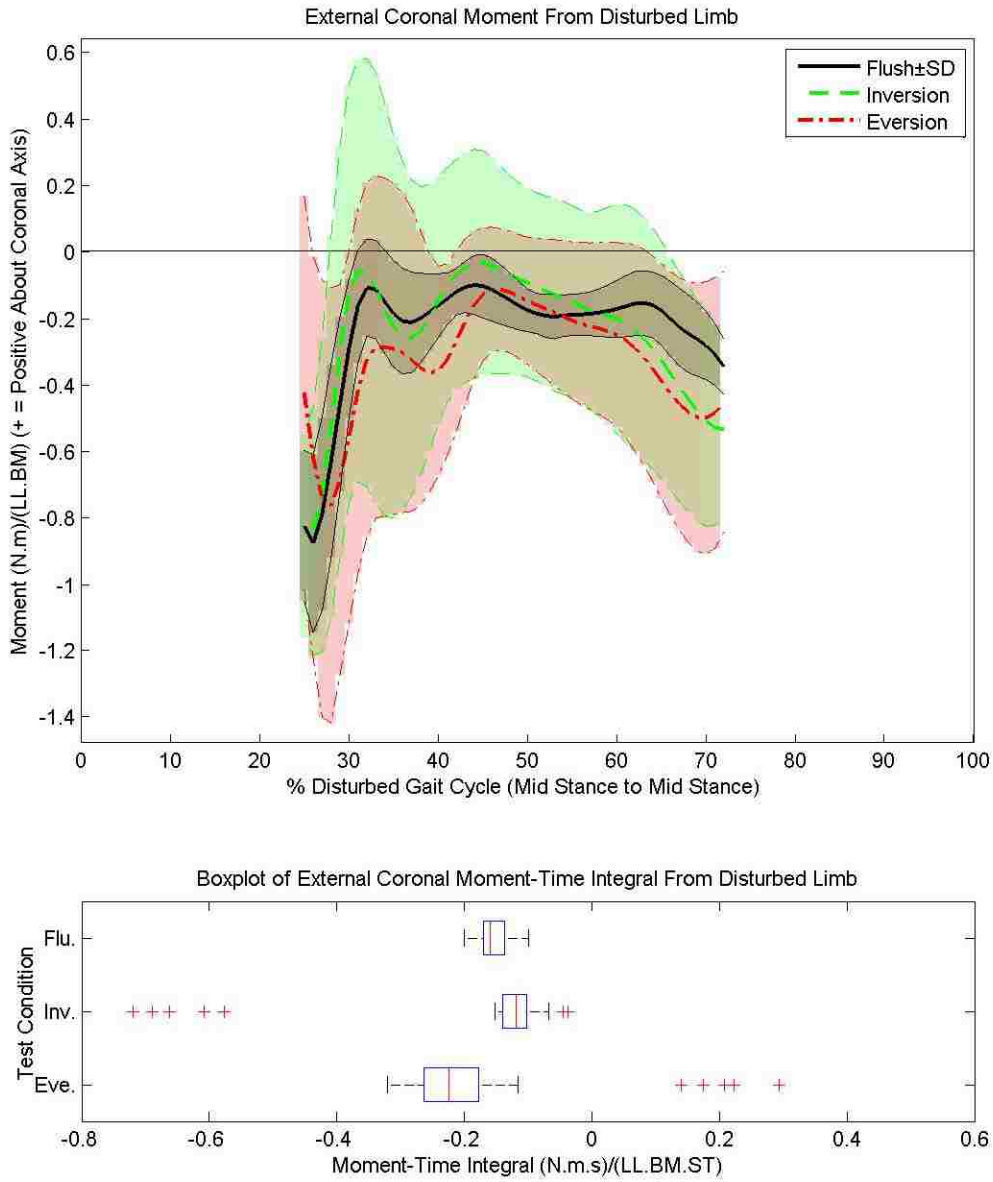

Figure 24 – Top: Time series of mean external coronal moment applied to the COM of the body by the disturbed limb for each condition over the disturbed gait cycle. Data only plotted during stance phase of the disturbed limb. Mean and standard deviation lines are for all trials for all participants. ***Bottom:*** Boxplot of time integral of external coronal moment applied to COM by the disturbed limb. Time series and boxplot data normalized to body mass (BM), leg length (LL), and stance time (ST).

Related to biomechanical hypothesis 1.6, these results reject the null hypothesis, and support the alternative hypothesis that the time integral of the external moment acting on the COM caused by the disturbed limb was not equivalent for all conditions. The eversion condition had a significantly more negative time integral than the inversion condition. This can be seen in row five of ***Table 2*** and ***Figure 24***. These results suggest that the disturbed limb was used to recover from the disturbance within the stance phase of the disturbed gait cycle. No significant difference was detected between the inversion and flush conditions or between the eversion and flush conditions. However, in viewing the time series plot and boxplot of ***Figure 24*** it can be seen that the time integral of the external moment acting on the COM caused by the disturbed limb for the eversion case was seemingly more negative than the flush case. A significant difference may not have been detected between this pair due to the high variance of this metric. It should be noted that the hip and external coronal moment-time integrals seem to share similar characteristics in that they both exhibit significant differences only between inversion and eversion. The observed outliers for these two metrics were from a single subject, whose biometric data (age, weight, height, gender) did not clearly distinguish them from the rest of the participants.

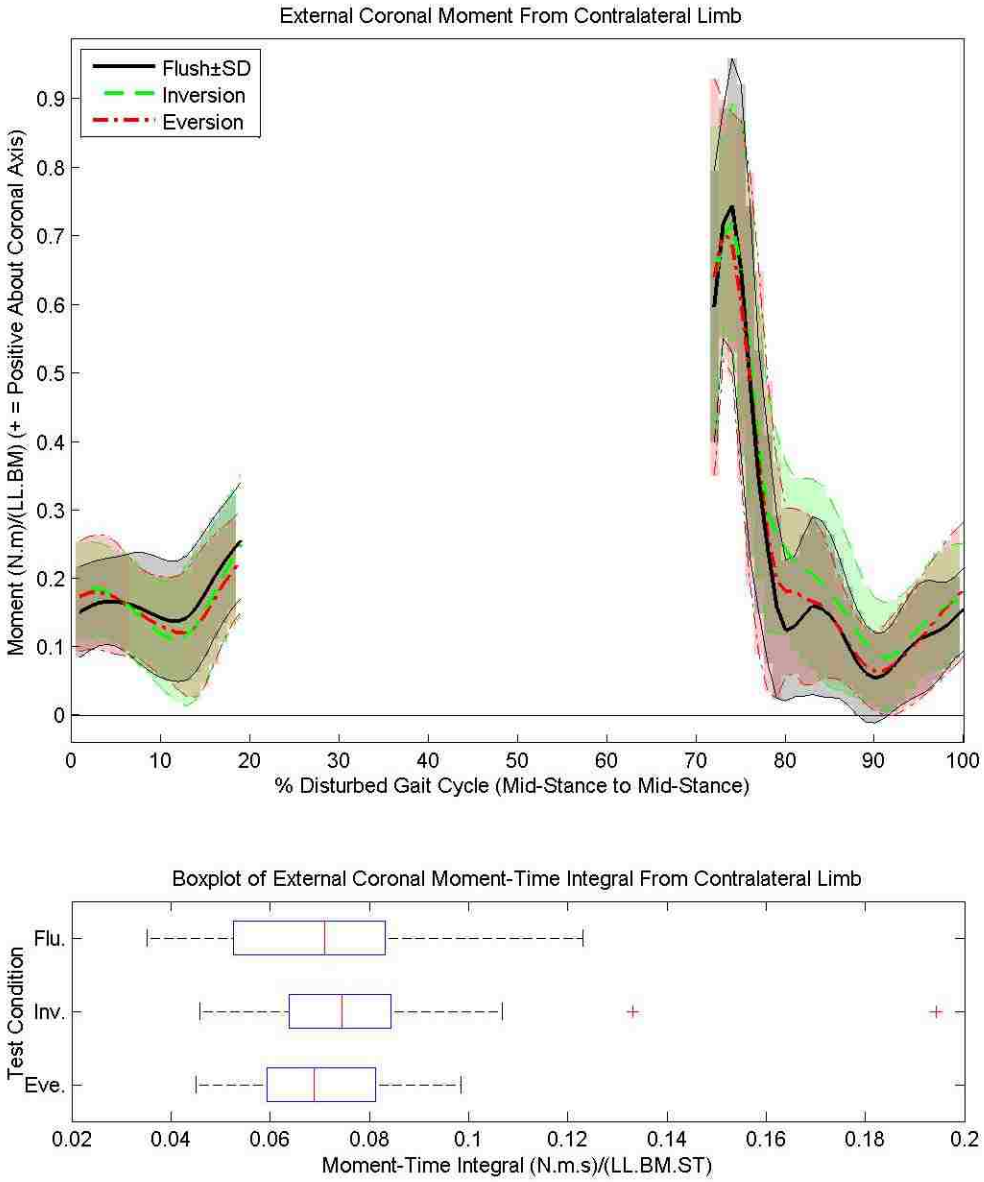

Figure 25 - Top: Time series of the mean external coronal moment applied to the COM of the body by the contralateral limb for each condition. Data only plotted during stance phase of the contralateral limb. ***Bottom:*** Boxplot of time integral of external coronal moment applied to COM by the contralateral limb. Time series and boxplot data normalized to body mass (BM), leg length (LL), and stance time (ST).

Related to biomechanical hypothesis 1.7, these results fail to reject the null hypothesis, and do not support the alternative hypothesis that the time integral of the external moment acting on the COM caused by the contralateral limb was not equivalent for all conditions. This can be seen in row six of ***Table 2*** and ***Figure 25***. In comparing the boxplots of ***Figure 24*** and ***Figure 25,*** it can be seen that the differences between conditions, relative to the IQR of each condition, was less for the external coronal moment-time integral of the contralateral limb, when compared to that of the disturbed limb. These results do not contradict the portion of biomechanical hypothesis I which states that the use of correction strategies within the disturbed gait cycle will be primarily carried out by the disturbed limb (during its stance phase).

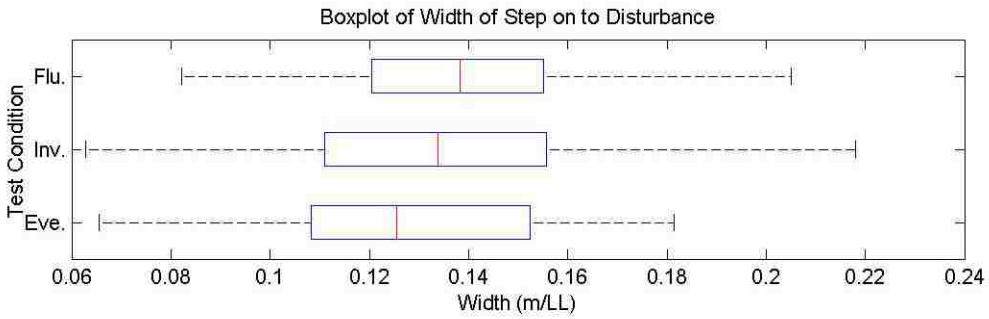

Figure 26 - Boxplot of time integral of the step width on to disturbance for all conditions. Boxplot data normalized to leg length (LL)

Related to biomechanical hypothesis 1.5, these results fail to reject the null hypothesis, and do not support the alternative hypothesis that the step width was not equivalent for all conditions. This can be seen in row seven of ***Table 2*** and **Figure 26**.

3.2 Biomechanical Hypothesis II Results

Statistical test results of performance metrics are displayed in ***Table 3***, and in general, support biomechanical hypothesis II, which was: "When adapting to coronally-uneven and unexpected terrain, the foot acts as a multi-segmented system in which the ankle, midtarsal, and the metatarsophalangeal joints each adapt to the uneven terrain." The hindfoot WRT tibia (AJ) coronal angle exhibited significant pairwise differences between all conditions at early-stance (ES), and between inversion and eversion at late-stance (LS), as seen in row one and two of ***Table 3***, which correspond to ***Figure 27***. The forefoot WRT hindfoot (MTJ) coronal angle exhibited a significant pairwise difference between the flush and eversion conditions at both ES and LS, as seen in row three and four of ***Table 3***, which correspond to ***Figure 28***. The MTJ coronal moment-time integral exhibited significant pairwise differences between all conditions, as seen in row five of ***Table 3***, which corresponds to ***Figure 29***. However, statistical testing of the hallux WRT forefoot (MPJ) coronal moment-time integral did not support that it was not equal between conditions, as seen in row six of ***Table 3***, which corresponds to ***Figure 30***.

Metric	Units	P-Value	Median (IQR)			Condition Differences		
			Flush	Inversion	Eversion	F to I	F to E	I to E
Hindfoot WRT Tibia (AJ) ES Coronal Angle	Degrees	< 0.001	-4.11(3.21)	7.52(5.55)	-13.44(4.37)	F < I	F > E	I > E
Hindfoot WRT Tibia (AJ) LS Coronal Angle	Degrees	< 0.001	-2.57(2.95)	3.37(4.54)	-7.04(3.97)	No Sig Diff	No Sig Diff	I > E
Forefoot WRT Hindfoot (MTJ) ES Coronal Angle	Degrees	< 0.001	-0.19(2.21)	0.81(2.26)	-2.37(2.16)	No Sig Diff	F > E	I > E
Forefoot WRT Hindfoot (MTJ) LS Coronal Angle	Degrees	< 0.001	0.76(2.36)	3.31(3.04)	-3.73(3.78)	No Sig Diff	F > E	I > E
Forefoot WRT Hindfoot (MTJ) Coronal Moment-Time Integral	$\frac{N \cdot m \cdot s}{BM \cdot LL \cdot ST}$	< 0.001	0.03(0.05)	-0.07(0.04)	0.13(0.06)	F > I	F < E	I < E
Hallux WRT Forefoot (MPJ) Coronal Moment-Time Integral	$\frac{N \cdot m \cdot s}{BM \cdot LL \cdot ST}$	0.619	0.04(0.02)	0.03(0.02)	0.03(0.02)	No Sig Diff	No Sig Diff	No Sig Diff

Table 3 - Statistical results for biomechanical hypothesis II. P-values based on Friedman test. Pairwise differences based on Wilcoxon signed-rank tests, with a Bonferroni correction, and an alpha level of 0.05. Metrics normalized to body mass (BM), body height (BH), leg length (LL), and stance time (ST). Early-stance (ES), and late-stance (LS) time points used for angle metrics. Median and interquartile range (IQR) reported due to non-normal nature of metrics.

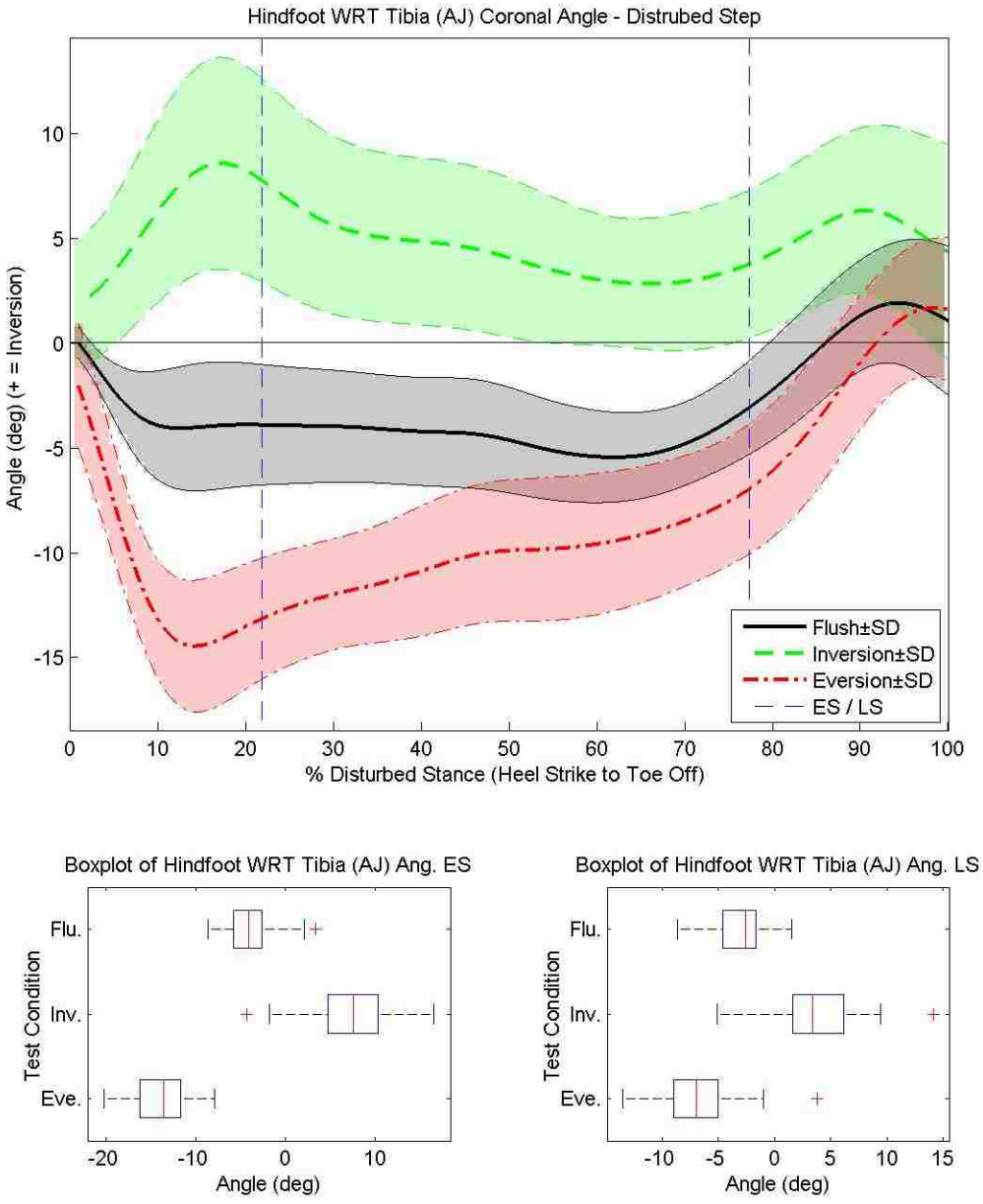

***Figure 27 - Top**:* Time series of mean hindfoot WRT tibia (AJ) coronal angle for disturbed step for each condition. Vertical dotted lines indicate average early-stance (ES) and late-stance (LS) time points. Mean and standard deviation lines are for all trials for all participants. ***Bottom Left**:* Boxplot of AJ angle for each condition at ES. ***Bottom Right**:* Boxplot of AJ angle for each condition at LS.

Related to biomechanical hypothesis 2.1, these results reject the null hypothesis, and support the alternative hypothesis that the coronal angle of the ankle joint (AJ) during early single limb stance of the disturbed limb was not equivalent for all conditions. In addition, the AJ coronal angle was significantly more positive for the inversion condition compared to the flush condition, and was significantly more negative for the eversion condition compared to the flush condition. This can be seen in ***Figure 27*** and in row one of ***Table 3.*** These results suggest that in early-stance, the AJ was experiencing coronal angular motion, and was adapting to the disturbance.

Related to biomechanical hypothesis 2.2 these results reject the null hypothesis, and support the alternative hypothesis that the coronal angle of the AJ during late single limb stance of the disturbed limb was not equivalent for all conditions. In addition, the AJ coronal angle was significantly more positive for the inversion condition compared to the eversion condition. This can be seen in ***Figure 27*** and in row two of ***Table 3.*** These results suggest that in late-stance, the AJ was experiencing coronal angular motion, and was adapting to the disturbance. It should be noted that in late-stance the differences between conditions appear smaller than in early-stance.

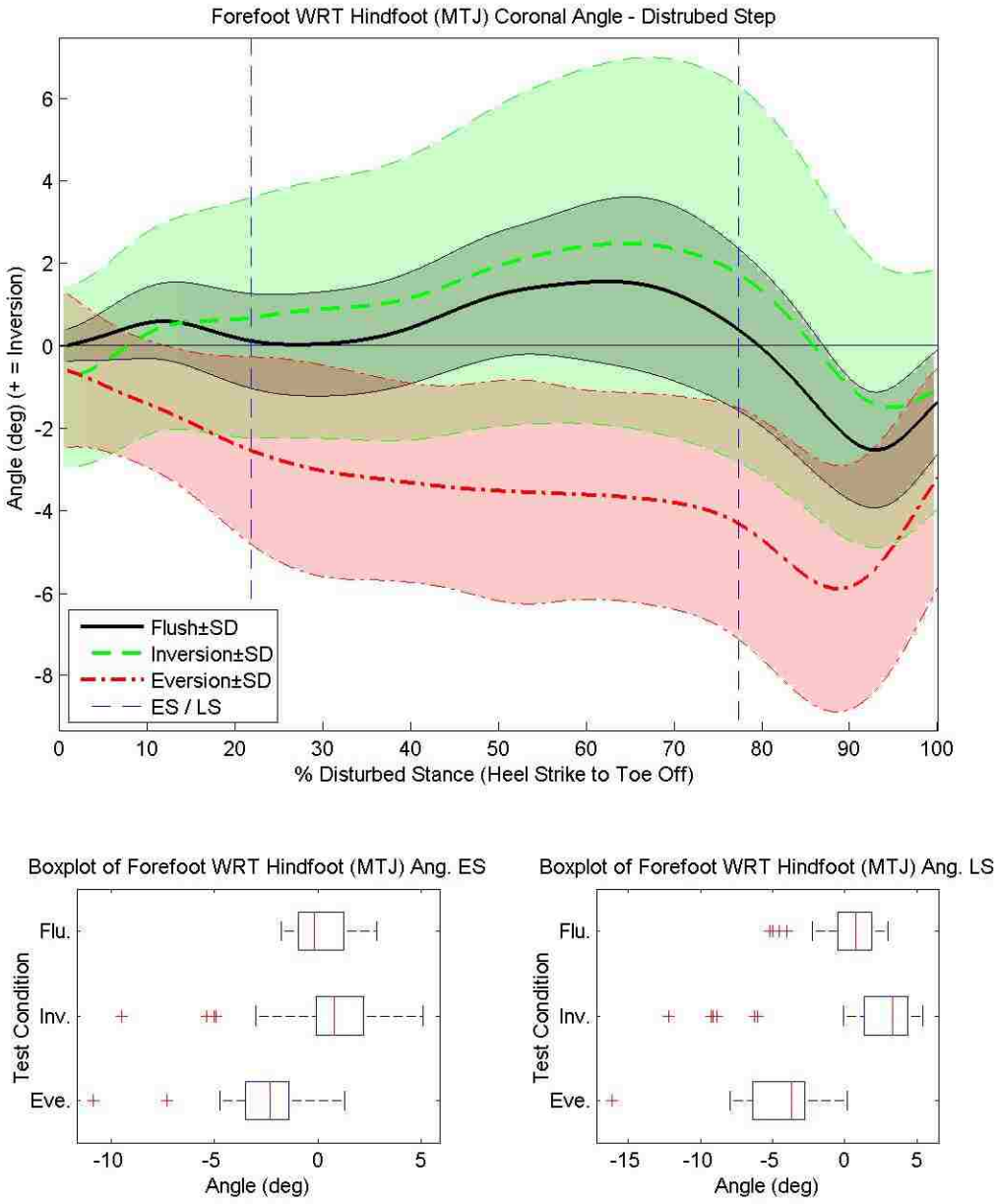

Figure 28- Top: Time series of mean forefoot WRT hindfoot (MTJ) coronal angle for disturbed step for each condition. Vertical dotted lines indicate average early-stance (ES) and late-stance (LS) time points. Mean and standard deviation lines are for all trials for all participants. ***Bottom Left****:* Boxplot of MTJ angle for each condition at ES. ***Bottom Right****:* Boxplot of MTJ angle for each condition at LS.

Related to biomechanical hypothesis 2.3, these results reject the null hypothesis, and support the alternative hypothesis that the coronal angle of the midtarsal joint (MTJ) during early single limb stance of the disturbed limb was not equivalent for all conditions. In addition, the MTJ coronal angle was significantly more negative for the eversion condition compared to both the flush condition and inversion condition. This can be seen in ***Figure 28*** and in row 3 of ***Table 3.*** These results suggest that in early-stance, the MTJ was experiencing coronal angular motion, and was adapting to the disturbance, particularly for the eversion condition.

Related to biomechanical hypothesis 2.4, these results reject the null hypothesis, and support the alternative hypothesis that the coronal angle of the MTJ during late single limb stance of the disturbed limb was not equivalent for all conditions. In addition, the MTJ coronal angle was significantly more negative for the eversion condition compared to both the flush condition and the inversion condition. This can be seen in ***Figure 28*** and in row four of ***Table 3.*** These results suggest that in late-stance, the MTJ was experiencing coronal angular motion, and was adapting to the disturbance, particularly for the eversion condition. The behavior of the MTJ in late-stance and early-stance appear to be similar, with the inversion condition closely following the flush condition, while the eversion condition was more negative than the flush and inversion conditions.

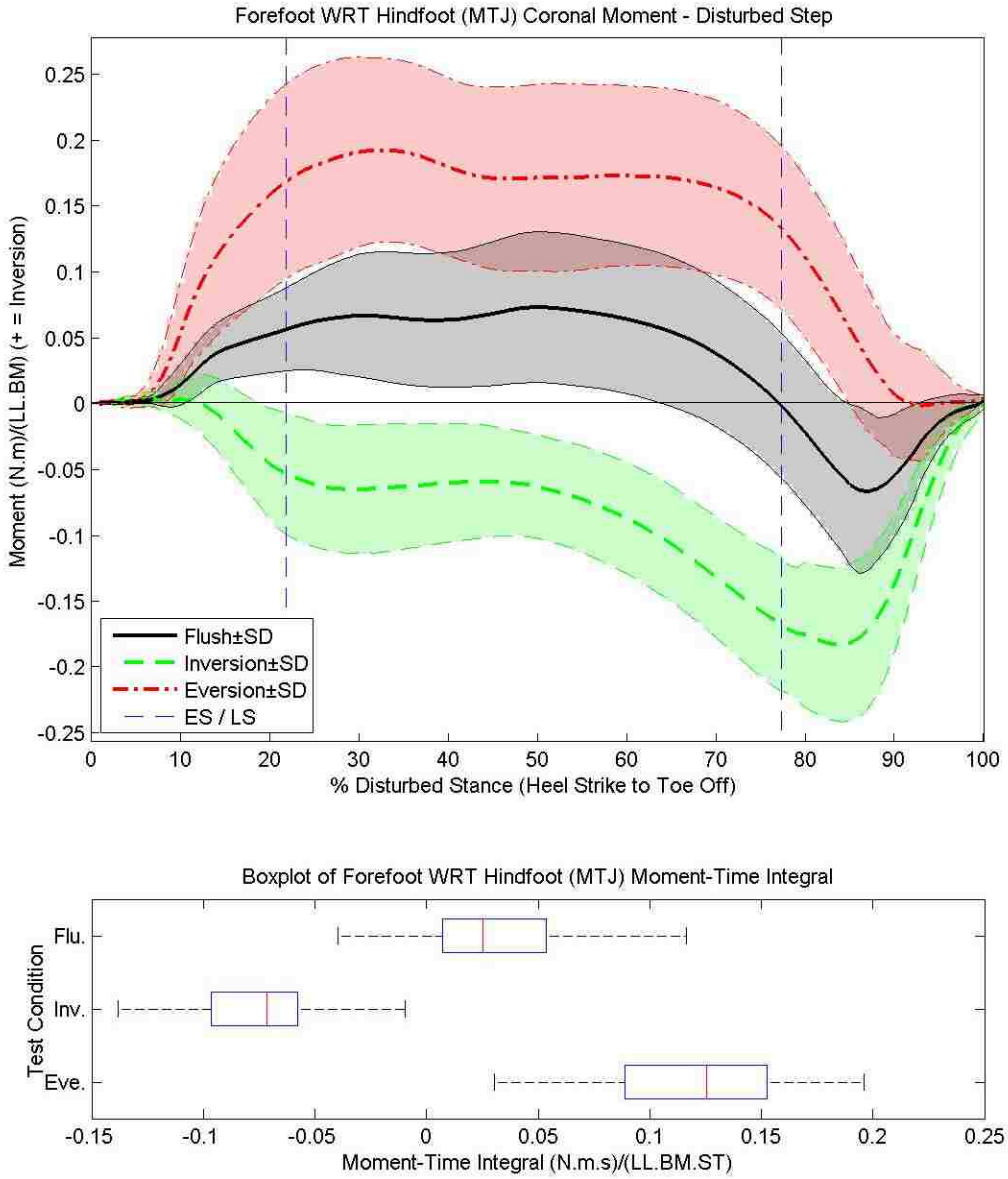

Figure 29 - Top: Time series of mean forefoot WRT hindfoot (MTJ) coronal moment for each condition. Vertical dotted lines indicate average early-stance (ES) and late-stance (LS) time points. Mean and standard deviation lines are for all trials for all participants. ***Bottom:*** Boxplot of time integral of MTJ coronal moment. Time series and boxplot data normalized to body mass (BM), leg length (LL), and stance time (ST).

Related to biomechanical hypothesis 2.5, these results reject the null hypothesis, and support the alternative hypothesis that the time integral of the coronal moment of the midtarsal joint (MTJ) was not equivalent between all conditions. In addition, the MTJ coronal moment-time integral was significantly more negative for the inversion condition compared to the flush condition, and was significantly more positive for the eversion condition compared to the flush condition. This can be seen in in ***Figure 29*** and in row five of ***Table 3***. These results suggest that the MTJ coronal moments were different between terrain conditions, and that the joint moment was adapting to each condition. Throughout stance, the MTJ moment was more negative for the inversion condition compared to the other two conditions, and was more positive for the eversion condition compared to the other two conditions.

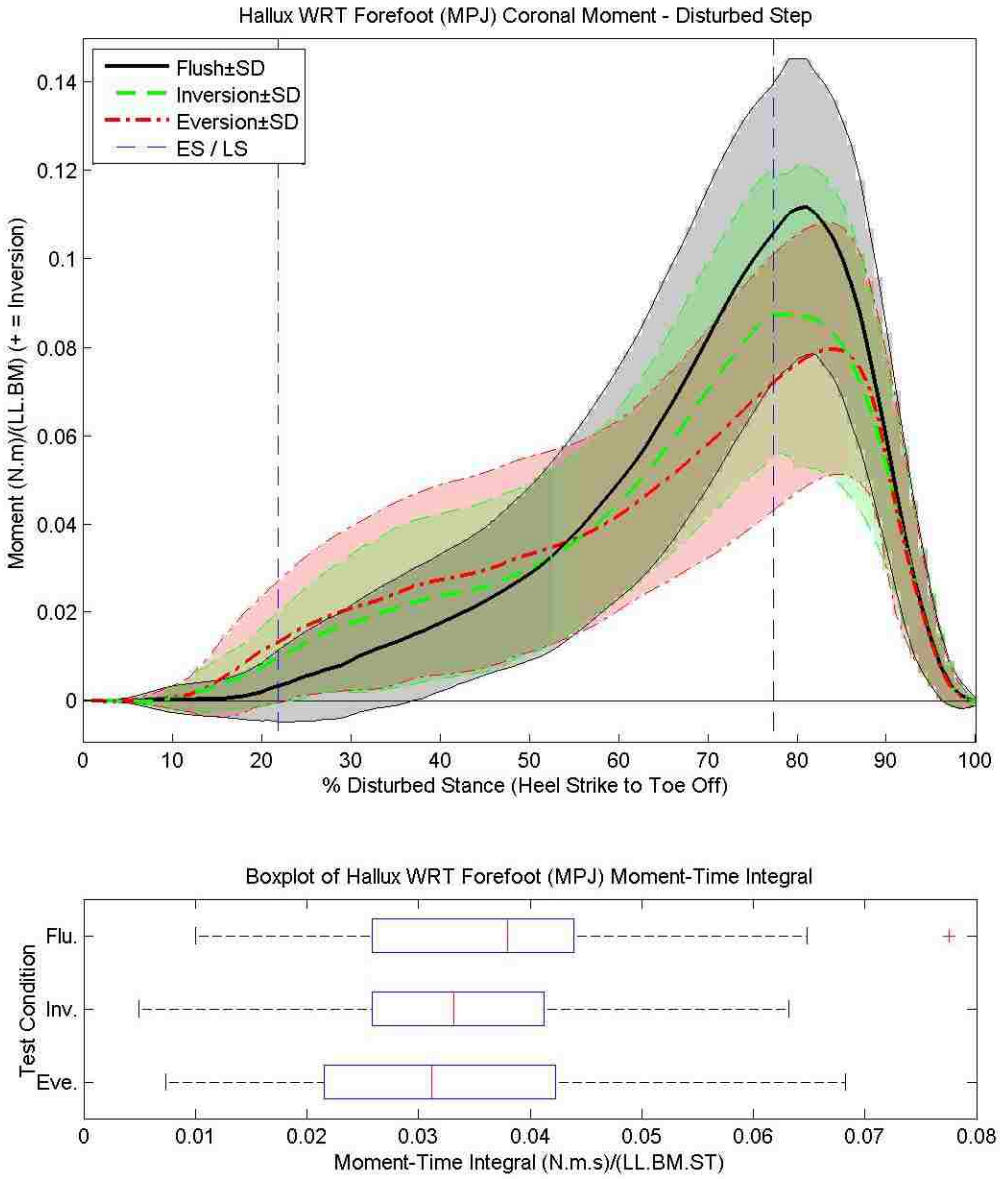

Figure 30 - Top: Time series of mean hallux WRT forefoot joint (MPJ) coronal moment for each condition. Vertical dotted lines indicate average early-stance (ES) and late-stance (LS) time points. Mean and standard deviation lines are for all trials for all participants. ***Bottom:*** Boxplot of time integral of MPJ coronal moment. Time series and boxplot data normalized to body mass (BM), leg length (LL), and stance time (ST).

Related to biomechanical hypothesis 2.6, these results fail to reject the null hypothesis, and do not support the alternative hypothesis that the time integral of the coronal moment of the metatarsophalangeal joint (MPJ) was not equal for all conditions. This can be seen in ***Figure 30*** and in row six of ***Table 3.*** This suggests that the MPJ coronal moment did not differ between terrain conditions in a significant manner, and that its moment did not significantly adapt to the different conditions. It should be noted that there does appear to be a slightly reduced peak for both the inversion and eversion conditions; however, given the integral metric, this slight difference in peak values did not have a significant effect on the statistical tests.

Chapter IV: Discussion

4.1 Interpretation

4.1a Biomechanical Hypothesis I Interpretation

The experimental device in the eversion condition appears to have disturbed the gait of the participants tested. Minimum inclination angles were significantly less for the eversion condition when compared to the flush condition, indicating reduced participant stability in eversion (see row two of ***Table 2*** and ***Figure 21***). The range of the inclination angles for the flush condition agrees with the range previously observed for stable walkers [11]. The range of normalized coronal angular momentum for the flush condition also agrees with the range previously reported for stable walkers [12, 13]. The range of coronal angular momentum was greater for the eversion condition when compared to inversion and flush conditions, indicating reduced participant stability [12] in eversion (see row one of ***Table 2*** and ***Figure 20***). The eversion condition exhibited a range of coronal angular momentum similar to that of amputee walkers [12]. That the eversion condition reduced the stability of intact participants to that of amputees, who have been shown to fall more [54], supports that the disturbance had a clinically meaningful effect on gait. That both stability metrics (minimum inclination angle and range of coronal angular momentum) exhibited significant differences between eversion and flush conditions, but not inversion and flush conditions, strongly suggests that the eversion condition had the greater destabilizing effect on gait stability.

Nearly all mediolateral stability metrics, including the two chosen for this study, are affected by the external coronal moment that each lower limb applies to the COM of the participant. To determine which limbs were being used by the participants to recover from the disturbance, the external coronal moment-time integrals of the disturbed and contralateral limbs were analyzed. Statistical testing detected that the external coronal moment-time integral of the disturbed limb was not equal between all conditions, but did not detect that the external coronal moment-time integral of the contralateral limb was not equal between all conditions (see rows five and six of ***Table 2, Figure 24, Figure***

25). That the disturbed limb's moment-time integral was not equal between all conditions suggests that it was adapting to the terrain conditions. That a difference was not detected between conditions for the contralateral limb suggests that it was adapting less to the terrain conditions. In addition, compared to the contralateral limb, the disturbed limb's moment-time integral had magnitudes, which were two to three times larger, which indicates that it had a larger effect on the range of coronal angular momentum (see ***Equation 2***). The disturbed limb's adaptation to each condition, as well as the relatively large magnitude of its moment-time integral, suggest that it, as opposed to the contralateral limb, was primarily used to recover from the disturbance.

To determine which recovery mechanisms were being employed by the disturbed limb, metrics indicating the use of the stepping, ankle, and hip strategies were compared. Due to the unexpected (blinded) nature of the disturbance conditions analyzed, participants could not implement the stepping strategy on to the disturbance device. Supporting this statement was the fact that statistical testing did not reject the null hypothesis that the step width was the same for all conditions (see row seven of **Table 2** and **Figure 26**). While the stepping, hip, and ankle strategies may have been used by the contralateral limb, their contribution to the overall recovery was considered small relative to that of the disturbed limb, as evidenced by the lack of statistical evidence supporting that the coronal moment-time integral of the contralateral limb was different between conditions.

The ankle strategy of the disturbed limb was used for all conditions, as evidenced by the fact that the ankle moment of the disturbed limb exhibited significantly different time integrals for each of the three conditions tested (see row three of ***Table 2,*** and ***Figure* 22**). The shape and magnitude of the of the ankle moment curves calculated for all conditions agree with published results for straight line walking [17]. In response to the inversion condition, the ankle moment became more negative (considered an eversion moment) compared to the flush condition; and in response to the eversion condition the ankle moment became more positive (considered an inversion moment) compared to the flush condition. The purpose of a more positive (inverted) moment was to shift the COP

more medially, and the purpose of a more negative (everted) moment was to shift the COP more laterally [10]. By altering the COP, the ankle strategy affected both the inclination angle, and the range of coronal angular momentum, thus indicating its role in gait stability.

Contributing to the inversion moment about the ankle were most likely the muscle tibialis posterior. It is possible that at the limits of eversion, an inversion moment was produced by the medial ligament of the ankle, and by articular cartilage contact forces of the tibiotalar, and subtalar joints. Contributing to the eversion moment about the ankle were most likely the muscles peroneus longus and peroneus brevis. It is possible that at the limits of inversion an eversion moment was produced by the lateral ligament of the ankle, and by articular cartilage contact forces of the tibiotalar, and subtalar joints [48, 55].

The hip strategy was also used, as evidenced by the fact that statistical testing detected that the hip coronal moment-time integral was not equivalent for all conditions, and was significantly different between inversion and eversion conditions (see row four of ***Table 2, Figure 23***). In addition, by careful observation of the time series and boxplot of ***Figure 23***, it can be seen that the behavior of the hip moment in eversion is different than that of the flush and inversion conditions in that it has reduced peaks and is generally more positive. Contributing to the adduction moment about the hip were most likely the muscles adductor magnus, adductor longus, adductor brevis, pectineus and gracilis. Contributing to the abduction moment about the hip were most likely the muscles gluteus medius, gluteus minimus, tensor fasciae latae, and sartorius [48, 55].

That participants used the hip strategy in an observationally different way for eversion, and that participants' gait was more disturbed for the eversion condition, may both be related to the asymmetrical anatomy of the ankle joint [47]. It has been shown that the ankle joint has more ROM in inversion (~20°) than eversion (~10°) [54, 55]. Because the angle of the uneven disturbance was 15°, it is possible that at some point during the disturbed stance phase, the ankle joint complex reached its ROM limit in the

eversion condition. In this case, the ability of the ankle strategy to accurately control its COP would be hindered. To maintain balance, it is possible that the hip strategy was then used to shift the COM, thus affecting the inclination angle and range of coronal angular momentum. This hierarchical behavior, in which the ankle strategy was used for small coronal disturbances, and the hip strategy was used for larger disturbances, agrees with previously published studies [10, 17].

4.1b Biomechanical Hypothesis II Interpretation

The MSFM moment and angle curves for the flush condition agree well in terms of shape and magnitude with the original model literature for barefoot walking [25, 33]. The differences between the inversion and eversion disturbances on the joint angle curves for both the AJ and MTJ were up to 100% larger than those previously reported from cross-slope walking studies [30]. The larger differences were most likely due to an increased slope angle (15° instead of 10°), the unexpected nature of the disturbance used in this study, the use of a single disturbance as opposed to a continuous slope, and possibly the fact that a different MSFM was used.

Kinematics

The hindfoot WRT tibia (AJ) angle conformed in the coronal plane to the surface of the disturbance in an asymmetric manner in early-stance, as seen in row one of ***Table 3*** and ***Figure 27***. It is assumed, based on anatomical descriptions [47, 55], that the inversion and eversion measured occurred at the subtalar joint, and that dorsiflexion and plantarflexion occurred at the tibiotalar joint, both of which were captured in the AJ definition used for this study. The differences observed in AJ coronal angles between conditions appeared to be slightly larger in early-stance when compared to late-stance. In early-stance, the AJ coronal angle also exhibited a larger difference between the flush and inverted conditions, than between the flush and everted conditions. This result agrees with previous studies which have shown the AJ to have a greater ROM in inversion compared to eversion [56, 57]. This result also agrees with evolutionary studies which

suggest that *Homo sapiens* inherited a larger ROM in ankle inversion from arboreal primate ancestors, whose feet best grasped branches in an inverted position [47].

Similar to the AJ, the forefoot WRT hindfoot (MTJ) angle conformed to the nature of the disturbance in an asymmetric manner (see rows three and four of ***Table 3*** and ***Figure 28***). It appears that the MTJ conformed more for the eversion condition, when compared to the inversion condition, both in early and late-stance. This may be related to the previously discussed asymmetrical ROM of the AJ. It is possible that in order for the forefoot to fully conform to the surface of the disturbance, the MTJ had to evert more in the eversion condition to compensate for the AJ's relatively small amount of eversion adaptation.

It is possible to attribute the observed asymmetries in foot adaptations to the coronally-uneven terrain to the oblique and multi-axis nature of the AJ [58 - 60], and to the midtarsal joint locking mechanism [61]. It has been suggested that these features of the foot and ankle are evolutionary adaptations that maximize the efficiency of *Homo sapiens* gait [47]. Of the two joints that comprise the AJ, the tibiotalar and subtalar joints, the subtalar joint exhibits an oblique axis [58], which has been shown to couple inversion of the foot with plantarflexion and internal rotation (known as supination), and to couple eversion of the foot with dorsiflexion and external rotation (known as pronation) [55], [59]. Lewis reasoned that some of this coupling could be related to the body's lateral sway of COM at the early-stance of gait, and its medial sway at late-stance [62]. This coupling provides an explanation for the hindfoot's tendency in all conditions to invert in late-stance (see ***Figure 27***), which was when the foot was plantar flexed, a position that is coupled to inversion.

The midtarsal joint locking mechanism may explain the differences of the MTJ kinematics between inversion and eversion disturbances. The midtarsal joint locking mechanism closely packs the talus, calcaneus, navicular, cuboid, cuneiforms, and metatarsals during push off (when the foot is plantar flexed and slightly inverted), thereby stiffening the foot and increasing the efficiency of the ankle moment's transfer of power

to the ground [55, 61]. In cadaveric studies, it has been shown that while the subtalar joint is inverted, the ROM of the first and fifth metatarsals in dorsiflexion to plantarflexion (relative to the tibia) is significantly reduced, when compared to the everted case [61]. A somewhat similar behavior was observed in this study, as the coronal angle of the MTJ at ES and LS, which was measured by the sagittal plane motion of the first and fifth metatarsals, deviated less from the flush condition for the inversion condition (when the calcaneus was inverted) when compared to the eversion condition (when the calcaneus was everted). See rows three and four of ***Table 3*** and ***Figure 28***.

Kinetics

The AJ moment values were the same as those previously reported under the title "Ankle Coronal Moment" in biomechanical hypothesis I (see row three of ***Table 2*** and ***Figure 22***). The two moments were identical because the AJ moment was defined as the hindfoot WRT tibia moment, and this moment incorporated the forces and moments from the hindfoot, forefoot and hallux sections, which comprised the whole foot. Both moments were also with respect to the tibia, making their frame of reference identical.

The existence of an observational difference between the AJ coronal moment-time integral data (see row three of ***Table 2*** and ***Figure 22***) and the MTJ coronal moment-time integral data (see row five of ***Table 3*** and ***Figure 29***) suggests the hindfoot had more functionality than simply transferring moments to the forefoot and hallux sections. This is particularly true in early-stance, as the hindfoot bore a significant portion of the total force being applied to the foot (see ***Figure 13***). It can be reasoned that during this period, moments applied to the hindfoot had an influence over the overall COP of the foot. Coronal moments acting on the hindfoot, which were not transferred through the MTJ, were most likely caused by ligament connections to the tibia and fibula, forces from tendons that did not insert into the hindfoot bones, and articular cartilage contact forces of the AJ. The major AJ ligaments affecting coronal plane motion were the lateral and medial ligament groups of the ankle [48]. Tendons which did not connect directly to the hindfoot, but may have applied forces through their synovial sheaths would have been the

peroneus longus and brevis on the lateral side; and the flexor digitorum longus, flexor hallucis longus, and tibialis posterior on the medial side [48]. Due to its central insertion on the calcaneus, the coronal moment contribution of the Achilles tendon on the hindfoot is unclear.

In late-stance, the forefoot and hallux sections had the most influence over the COP of the foot. This is supported by the fact that the forefoot and hallux bore a significant portion of the total force being applied to the foot in late-stance (see ***Figure 13***). In addition, a significant difference in MTJ moment-time integrals for each of the terrain conditions exist, indicating it was adapting to the terrain. In late-stance, the role of the hindfoot changed, as it could no longer directly influence the COP because it was not in contact with the ground. Instead, it acted as a link between the tibia and the forefoot sections, allowing the COP to move anterior to the hindfoot, and also transferring coronal moments between the forefoot and the tibia.

One of the main contributors to the forefoot coronal moment were likely the leg muscles. The tibialis posterior likely provided inversion moments, while the peroneus longus and peroneus brevis likely provided eversion moments [48, 55]. Helping to transfer the coronal moments across the MTJ to the hallux section were most likely the articular cartilage contact forces created by the midtarsal locking mechanism, the numerous ligaments connecting the hindfoot and forefoot sections, and the internal muscles of the foot.

Viewing the coronal moments of the MPJ (see row six of ***Table 3*** and ***Figure 30***) no major difference in the moment curves between the conditions were observed, except a slightly reduced peak for both disturbed conditions. That the moment-time integral between conditions was not significantly different (see row six of ***Table 3***) supports that the MPJ did not significantly adapt its moment in the coronal plane when encountering uneven terrain. Instead, the moments applied to the hallux section by internal and external forces seem to be similar across conditions.

An interesting observation is that the kinetic adaptations of the foot in the coronal plane were noticeably more symmetric than the kinematic adaptations. That is to say that for the AJ and MTJ the amount that the disturbed moment curves deviate from the flush condition are roughly equal and opposite (compare row three of ***Table 2*** with row five of ***Table 3*** and ***Figure 22*** with ***Figure 29***). This makes sense, as the disturbance itself was symmetric, and ultimately it was the kinetic adaptations of the body which were used to maintain stability [10, 17]. From this observation, it may be argued that kinematic adaptations of the foot were carried out in an asymmetric manner to accommodate the body's anatomical constraints, and in doing so, provided the necessary positioning of each foot segment to achieve the desired corrective kinetic adaptations.

4.2 Implications

The findings of this study are particularly relevant to the prosthetic research community, and suggest prosthetic devices could benefit from AJs and MTJs that adapt to coronally-uneven terrain. Prosthetic devices to date only offer simple, spring-like adaptations in the coronal plane of the AJ and MTJ. However, the findings of this study, when coupled with existing modeling results [12-14], suggest more advanced and active control of these joints in the coronal plane may be required to maintain balance on unexpected and coronally-uneven terrain during gait. With such improved devices, it may even be possible to increase the balance performance of amputees over that of non-amputee participants on specific types of unexpected and coronally-uneven terrain. This may be achieved by developing a prosthetic ankle with a greater eversion ROM than the human ankle. This could reduce the need for amputees to compensate for eversion disturbances with the hip strategy, which, in this study, seemed to be less effective for intact participants than the ankle strategy.

In the field of orthopedics, this study may help improve the patient outcomes of commonly prescribed lower-limb interventions. In particular, the findings of this study suggest that procedures that reduce patients' ROM of the foot and ankle in the coronal plane may reduce their stability on unexpected and coronally-uneven terrain. Ankle

braces, ankle arthrodesis, and ankle arthroplasty are examples of orthopedic procedures that have been shown to reduce AJ ROM [63, 64]. While it may not be possible to restore patients' full ROM for all of these procedures, the fact that doing so may improve patient stability on unexpected and coronally-uneven terrain, and thereby reduce the risk of falling, should be considered when weighing intervention options. This consideration would be particularly important for more active patients who may encounter unexpected and coronally-uneven terrain on a regular basis, and would therefore potentially receive the most benefit from a non-limited ROM intervention.

4.3 Limitations

One limitation of this study was the step down between the disturbance device and the rest of the walkway. The step down was 0.7cm and 2.7cm for the flush and the inverted/everted conditions, respectively. Great effort was made to minimize these values, as it was recognized that test metrics were measuring both the effects of an inversion/eversion and a slight step down. However, the step down could not be eliminated completely as it was a byproduct of keeping the entire disturbance device below the walkway surface to enable the blinding of participants to the condition of the device. It was also recognized that in real-world conditions individuals are may also experience a slight step down when encountering uneven terrain, such as dips in a field, or curbs from a sidewalk to a street. Additionally, the step down was symmetric for both disturbance conditions, therefore differences observed between the two conditions could be attributed to the angle, and not the height, of the disturbance.

A second limitation was the limited amount of biometric data collected on each of the participants, and the gender imbalance of the participant population. In light of the existence of outliers, specifically regarding the coronal moment-time integral of the hip and contralateral limb, more participant biometric data may have been used to determine the cause of these outliers. One such piece of data could have been foot type, specifically arch type and degree of pronation. Also, due to the fact that only one participant was female, a significant portion of the target population was under-represented in this study.

Another limitation of this study was the validation of the proportionality assumption and the multi-segment foot modeling technique was only performed on flat ground. It has been suggested that shear forces do not necessarily act about the COP of the foot [32], which is as assumption made by the MSFM chosen for this study. It may be possible that this error increases in the inverted and everted conditions of this study, where the overall shear forces in the medial and lateral directions increase. However, while shear forces are larger under these conditions, analysis revealed that the vertical component of the GRF remained the largest contributor to the coronal moments of each segment.

It was also assumed, in biomechanical hypothesis I, that if a difference was detected between conditions in the external coronal moment-time integral of the disturbed limb, and not in the external coronal moment-time integral of the contralateral limb, that use of the hip and ankle strategies within the disturbed step were the primary recovery mechanisms. It is important to note that a difference not being detected in the external coronal moment-time integral of the contralateral limb does not mean that a difference did not exist. It is possible that the size of a difference that did exist between conditions was simply too small for detection given the sample size of this study. The same can be said for the step width metric, as a difference may have existed between conditions, but may not have been detected given the sample size used.

Finally, the analysis of only coronal plane moments could be considered a limitation of this work. It has been shown that sagittal plane instability and lateral plane instability are nearly decoupled from a controls perspective [14]; however, it is possible that sagittal and transverse plane joint moments played an important role in the control of coronal plane motion. Analysis of the effects of sagittal and transverse plane joint moments on coronal plane stability was beyond the scope of this work, and will be addressed in future work.

4.4 Future Work

Future work on this project will be focused on two areas: further analyzing already collected data, and using current data analysis to inform the design of future prosthetic interventions. There are a multitude of interesting questions to be asked about the dynamic adaptation of the body to the coronally-uneven terrain. One such question is how the different joints interact with one another to maintain stability, and how the body decides in which joint the stability effort should be maximized. Another important topic is the difference between the blinded and unblinded responses of the participants to the disturbance. Finally, as previously mentioned, it would be interesting to understand whether coronal plane moments are the primary adaptation to coronally-uneven terrain, or if sagittal and transverse plane moments also play a significant role in maintaining stability.

The second focus of future work will be on using existing data analysis, as well as newly collected amputee participant data, to design and build a prosthetic intervention for transtibial amputees. The first part of this goal will be establishing the baseline performance of amputee participants as they perform the same experiment that the non-amputee participants did. Once this is complete, it will be possible to compare and contrast the performance of the amputee and non-amputee populations, which will highlight where current prosthetic devices fall short. With this information, a mathematical model will be developed for a mechanical device that can mimic, and perhaps improve upon, the observed behavior of non-amputee participants. This device will consist of both passive, and actively controlled elements, which will necessitate the use of sensors and the development of control algorithms. A subset of amputee participants will be outfitted with a prototype device in the lab, and will be asked to perform the same experiment as they did with their previous prosthetic device. Hopefully, the new device will improve the stability of amputee participants, and bring it to the same level of performance as non-amputee individuals when encountering unexpected and coronally-uneven terrain.

References

[1] D. A. Sleet, D. B. Moffett, and J. Stevens, "CDC's research portfolio in older adult fall prevention: a review of progress, 1985-2005, and future research directions," *J. Safety Res.*, vol. 39, no. 3, pp. 259–267, 2008.

[2] N. Niino, S. Tsuzuku, F. Ando, and H. Shimokata, "Frequencies and circumstances of falls in the National Institute for Longevity Sciences, Longitudinal Study of Aging (NILS-LSA)," *J Epidemiol*, vol. 10, pp. S90–S94, 2000.

[3] M. L. Finlayson and E. W. Peterson, "Falls, Aging, and Disability," *Phys. Med. Rehabil. Clin. N. Am.*, vol. 21, no. 2, pp. 357–373, May 2010.

[4] E. F, H. Tj, and T. Ra, "Economic dimensions of slip and fall injuries.," *J. Forensic Sci.*, vol. 41, no. 5, pp. 733–746, Sep. 1996.

[5] J. A. Stevens, S. L. Teh, and T. Haileyesus, "Dogs and cats as environmental fall hazards," *J. Safety Res.*, vol. 41, no. 1, pp. 69–73, Feb. 2010.

[6] W. Li, T. H. M. Keegan, B. Sternfeld, S. Sidney, C. P. Quesenberry, and J. L. Kelsey, "Outdoor Falls Among Middle-Aged and Older Adults: A Neglected Public Health Problem," *Am. J. Public Health*, vol. 96, no. 7, pp. 1192–1200, Jul. 2006.

[7] J. L. Kelsey, E. Procter-Gray, M. T. Hannan, and W. Li, "Heterogeneity of Falls Among Older Adults: Implications for Public Health Prevention," *Am. J. Public Health*, vol. 102, no. 11, pp. 2149–2156, Sep. 2012.

[8] S. E. Lamb, E. C. Jørstad-Stein, K. Hauer, C. Becker, and Prevention of Falls Network Europe and Outcomes Consensus Group, "Development of a common outcome data set for fall injury prevention trials: the Prevention of Falls Network Europe consensus," *J. Am. Geriatr. Soc.*, vol. 53, no. 9, pp. 1618–1622, Sep. 2005.

[9] T. M. Owings and M. D. Grabiner, "Step width variability, but not step length variability or step time variability, discriminates gait of healthy young and older adults during treadmill locomotion," *J. Biomech.*, vol. 37, no. 6, pp. 935–938, Jun. 2004.

[10] A. L. Hof, R. M. van Bockel, T. Schoppen, and K. Postema, "Control of lateral balance in walking: Experimental findings in normal subjects and above-knee amputees," *Gait Posture*, vol. 25, no. 2, pp. 250–258, Feb. 2007.

[11] C.-J. Chen and L.-S. Chou, "Center of mass position relative to the ankle during walking: A clinically feasible detection method for gait imbalance," *Gait Posture*, vol. 31, no. 3, pp. 391–393, Mar. 2010.

[12] A. K. Silverman and R. R. Neptune, "Differences in whole-body angular momentum between below-knee amputees and non-amputees across walking speeds," *J. Biomech.*, vol. 44, no. 3, pp. 379–385, Feb. 2011.

[13] H. Herr and M. Popovic, "Angular momentum in human walking," *J. Exp. Biol.*, vol. 211, no. 4, pp. 467–481, Feb. 2008.

[14] C. E. Bauby and A. D. Kuo, "Active control of lateral balance in human walking," *J. Biomech.*, vol. 33, no. 11, pp. 1433–1440, Nov. 2000.

[15] D. S. Marigold and A. E. Patla, "Gaze fixation patterns for negotiating complex ground terrain," *Neuroscience*, vol. 144, no. 1, pp. 302–313, Jan. 2007.

[16] D. Winter, "Human balance and posture control during standing and walking," *Gait Posture*, vol. 3, no. 4, pp. 193–214, Dec. 1995.

[17] C. D. MacKinnon and D. A. Winter, "Control of whole body balance in the frontal plane during human walking," *J. Biomech.*, vol. 26, no. 6, pp. 633–644, Jun. 1993.
[18] N. Matsusaka, "Control of the medial-lateral balance in walking," *Acta Orthop.*, vol. 57, no. 6, pp. 555–559, Jan. 1986.
[19] M. J. MacLellan and A. E. Patla, "Adaptations of walking pattern on a compliant surface to regulate dynamic stability," *Exp. Brain Res.*, vol. 173, no. 3, pp. 521–530, 2006.
[20] P. H. J. A. Nieuwenhuijzen and J. Duysens, "Proactive and Reactive Mechanisms Play a Role in Stepping on Inverting Surfaces During Gait," *J. Neurophysiol.*, vol. 98, no. 4, pp. 2266–2273, Oct. 2007.
[21] C. W. Linford, J. T. Hopkins, S. S. Schulthies, B. Freland, D. O. Draper, and I. Hunter, "Effects of Neuromuscular Training on the Reaction Time and Electromechanical Delay of the Peroneus Longus Muscle," *Arch. Phys. Med. Rehabil.*, vol. 87, no. 3, pp. 395–401, Mar. 2006.
[22] P. M. McAndrew, J. B. Dingwell, and J. M. Wilken, "Walking variability during continuous pseudo-random oscillations of the support surface and visual field," *J. Biomech.*, vol. 43, no. 8, pp. 1470–1475, May 2010.
[23] L. I. E. Oddsson, C. Wall III, M. D. McPartland, D. E. Krebs, and C. A. Tucker, "Recovery from perturbations during paced walking," *Gait Posture*, vol. 19, no. 1, pp. 24–34, Feb. 2004.
[24] S. B. Thies, J. A. Ashton-Miller, and J. K. Richardson, "What causes a crossover step when walking on uneven ground?: A study in healthy young women," *Gait Posture*, vol. 26, no. 1, pp. 156–160, Jun. 2007.
[25] D. A. Bruening, K. M. Cooney, and F. L. Buczek, "Analysis of a kinetic multi-segment foot model. Part I: Model repeatability and kinematic validity," *Gait Posture*, vol. 35, no. 4, pp. 529–534, Apr. 2012.
[26] B. A. MacWilliams, M. Cowley, and D. E. Nicholson, "Foot kinematics and kinetics during adolescent gait," *Gait Posture*, vol. 17, no. 3, pp. 214–224, Jun. 2003.
[27] J. Stebbins, M. Harrington, N. Thompson, A. Zavatsky, and T. Theologis, "Repeatability of a model for measuring multi-segment foot kinematics in children," *Gait Posture*, vol. 23, no. 4, pp. 401–410, Jun. 2006.
[28] J. Simon, L. Doederlein, A. S. McIntosh, D. Metaxiotis, H. G. Bock, and S. I. Wolf, "The Heidelberg foot measurement method: Development, description and assessment," *Gait Posture*, vol. 23, no. 4, pp. 411–424, Jun. 2006.
[29] C. Nester, R. K. Jones, A. Liu, D. Howard, A. Lundberg, A. Arndt, P. Lundgren, A. Stacoff, and P. Wolf, "Foot kinematics during walking measured using bone and surface mounted markers," *J. Biomech.*, vol. 40, no. 15, pp. 3412–3423, 2007.
[30] M. Damavandi, P. C. Dixon, and D. J. Pearsall, "Kinematic adaptations of the hindfoot, forefoot, and hallux during cross-slope walking," *Gait Posture*, vol. 32, no. 3, pp. 411–415, Jul. 2010.
[31] A. C. Novak, D. J. Mayich, S. D. Perry, T. R. Daniels, and J. W. Brodsky, "Gait Analysis for Foot and Ankle Surgeons— Topical Review, Part 2 Approaches to Multisegment Modeling of the Foot," *Foot Ankle Int.*, vol. 35, no. 2, pp. 178–191, Feb. 2014.

[32] M. Yavuz, G. Botek, and B. L. Davis, “Plantar shear stress distributions: Comparing actual and predicted frictional forces at the foot–ground interface,” *J. Biomech.*, vol. 40, no. 13, pp. 3045–3049, 2007.
[33] D. A. Bruening, K. M. Cooney, and F. L. Buczek, “Analysis of a kinetic multi-segment foot model part II: Kinetics and clinical implications,” *Gait Posture*, vol. 35, no. 4, pp. 535–540, Apr. 2012.
[34] M. Vukobratovic and B. Borovac, “Zero-Moment Point - Thirty Five Years of its Life,” *Int. J. Humanoid Robot.*, vol. 01, no. 01, pp. 157–173, Mar. 2004.
[35] M. Damavandi, P. C. Dixon, and D. J. Pearsall, “Ground reaction force adaptations during cross-slope walking and running,” *Hum. Mov. Sci.*, vol. 31, no. 1, pp. 182–189, Feb. 2012.
[36] M. P. Kadaba, H. K. Ramakrishnan, and M. E. Wootten, “Measurement of lower extremity kinematics during level walking,” *J. Orthop. Res.*, vol. 8, no. 3, pp. 383–392, May 1990.
[37] D. A. Winter, *Biomechanics and Motor Control of Human Movement*. John Wiley & Sons, 2009.
[38] “Inverse Dynamics - Visual3D Wiki Documentation.” [Online]. Available: http://www.c-motion.com/v3dwiki/index.php?title=Inverse_Dynamics. [Accessed: 25-Aug-2014].
[39] M. R. Pierrynowski and V. Galea, “Enhancing the ability of gait analyses to differentiate between groups: scaling gait data to body size,” *Gait Posture*, vol. 13, no. 3, pp. 193–201, May 2001.
[40] J. Rose and J. G. Gamble, *Human Walking*. Lippincott Williams & Wilkins, 2006.
[41] Kim HeungYoul, S. Sakurai, and Ahn JaeHan, “Errors in the measurement of center of pressure (CoP) computed with force plate affect on 3D lower limb joint moment during gait.,” *Int. J. Sport Health Sci.*, vol. 5, pp. 71–82, 2007.
[42] E. K. Antonsson and R. W. Mann, “The frequency content of gait,” *J. Biomech.*, vol. 18, no. 1, pp. 39–47, 1985.
[43] G. Di Giulio, N. Paone, G. L. Rossi, G. Miccoli, P. Christ, M. Geuder, A. Cristalli, R. Deboli, M. Valentino, and V. Rapisarda, “Measurement methods for the improvement of hand-arm vibrating testing: polymeric capacitive matrices and laser vibrometry applied to a hydraulic breaker,” in *Proc. of the 9 th Int. Conf. on Hand-Arm Vibration, Nancy, France*, 2001, pp. 5–8.
[44] T. D. Collins, S. N. Ghoussayni, D. J. Ewins, and J. A. Kent, “A six degrees-of-freedom marker set for gait analysis: Repeatability and comparison with a modified Helen Hayes set,” *Gait Posture*, vol. 30, no. 2, pp. 173–180, Aug. 2009.
[45] A. L. Bell, D. R. Pedersen, and R. A. Brand, “A comparison of the accuracy of several hip center location prediction methods,” *J. Biomech.*, vol. 23, no. 6, pp. 617–621, 1990.
[46] W. T. (Wilfrid T. Dempster, “Space requirements of the seated operator : geometrical, kinematic, and mechanical aspects of the body, with special reference to the limbs,” 1955.
[47] O. J. Lewis, “The joints of the evolving foot. Part I. The ankle joint.,” *J. Anat.*, vol. 130, no. Pt 3, pp. 527–543, May 1980.
[48] F. H. Netter, *Atlas of Human Anatomy*. Elsevier Health Sciences, 2010.

[49] P. C. Dixon, H. Böhm, and L. Döderlein, “Ankle and midfoot kinetics during normal gait: A multi-segment approach,” *J. Biomech.*, vol. 45, no. 6, pp. 1011–1016, Apr. 2012.
[50] S. H. Collins, P. G. Adamczyk, D. P. Ferris, and A. D. Kuo, “A simple method for calibrating force plates and force treadmills using an instrumented pole,” *Gait Posture*, vol. 29, no. 1, pp. 59–64, Jan. 2009.
[51] H. L. P. Hurkmans, J. B. J. Bussmann, E. Benda, J. A. N. Verhaar, and H. J. Stam, “Accuracy and repeatability of the Pedar Mobile system in long-term vertical force measurements,” *Gait Posture*, vol. 23, no. 1, pp. 118–125, Jan. 2006.
[52] C-Motion, “Force Structures,” *Force Structures*, 01-Jul-2013. .
[53] B. Vidakovic, *Statistics for Bioengineering Sciences: With MATLAB and WinBUGS Support*. Springer Science & Business Media, 2011.
[54] W. C. Miller, A. B. Deathe, M. Speechley, and J. Koval, “The influence of falling, fear of falling, and balance confidence on prosthetic mobility and social activity among individuals with a lower extremity amputation,” *Arch. Phys. Med. Rehabil.*, vol. 82, no. 9, pp. 1238–1244, Sep. 2001.
[55] S. Standring, *Gray’s Anatomy: The Anatomical Basis of Clinical Practice*. Churchill Livingstone/Elsevier, 2008.
[56] S. Dj and E. Jr, “Right to left differences in the ankle joint complex range of motion.,” *Med. Sci. Sports Exerc.*, vol. 26, no. 5, pp. 551–555, May 1994.
[57] S. B. Sepic, M. P. Murray, L. A. Mollinger, G. B. Spurr, and G. M. Gardner, “Strength and range of motion in the ankle in two age groups of men and women,” *Am. J. Phys. Med.*, vol. 65, no. 2, pp. 75–84, Apr. 1986.
[58] A. Lundberg, O. K. Svensson, G. Nemeth, and G. Selvik, “The axis of rotation of the ankle joint,” *J. Bone Joint Surg. Br.*, vol. 71-B, no. 1, pp. 94–99, Jan. 1989.
[59] A. Lundberg, O. K. Svensson, C. Bylund, I. Goldie, and G. Selvik, “Kinematics of the Ankle/Foot Complex—Part 2: Pronation and Supination,” *Foot Ankle Int.*, vol. 9, no. 5, pp. 248–253, Apr. 1989.
[60] K. A. Kirby, “Subtalar Joint Axis Location and Rotational Equilibrium Theory of Foot Function,” *J. Am. Podiatr. Med. Assoc.*, vol. 91, no. 9, pp. 465–487, Oct. 2001.
[61] C. B. Blackwood, T. J. Yuen, B. J. Sangeorzan, and W. R. Ledoux, “The Midtarsal Joint Locking Mechanism,” *Foot Ankle Int.*, vol. 26, no. 12, pp. 1074–1080, Dec. 2005.
[62] O. J. Lewis, “The joints of the evolving foot. Part II. The intrinsic joints.,” *J. Anat.*, vol. 130, no. Pt 4, pp. 833–857, Jun. 1980.
[63] H. B. Kitaoka, X. M. Crevoisier, K. Harbst, D. Hansen, B. Kotajarvi, and K. Kaufman, “The Effect of Custom-Made Braces for the Ankle and Hindfoot on Ankle and Foot Kinematics and Ground Reaction Forces,” *Arch. Phys. Med. Rehabil.*, vol. 87, no. 1, pp. 130–135, Jan. 2006.
[64] V. Valderrabano, B. Hintermann, B. M. Nigg, D. Stefanyshyn, and P. Stergiou, “Kinematic Changes After Fusion and Total Replacement of the Ankle Part 1: Range of Motion,” *Foot Ankle Int.*, vol. 24, no. 12, pp. 881–887, Dec. 2003.